

Adversarial Purification by Consistency-aware Latent Space Optimization on Data Manifolds

Shuhai Zhang*, Jiahao Yang*, Hui Luo, Jie Chen, Li Wang, Feng Liu, Bo Han, Mingkui Tan†

Abstract—Deep neural networks (DNNs) are vulnerable to adversarial samples crafted by adding imperceptible perturbations to clean data, potentially leading to incorrect and dangerous predictions. Adversarial purification has been an effective means to improve DNNs robustness by removing these perturbations before feeding the data into the model. However, it faces significant challenges in preserving key structural and semantic information of data, as the imperceptible nature of adversarial perturbations makes it hard to avoid over-correcting, which can destroy important information and degrade model performance. In this paper, we break away from traditional adversarial purification methods by focusing on the clean data manifold. To this end, we reveal that samples generated by a well-trained generative model are close to clean ones but far from adversarial ones. Leveraging this insight, we propose Consistency Model-based Adversarial Purification (CMAP), which optimizes vectors within the latent space of a pre-trained consistency model to generate samples for restoring clean data. Specifically, 1) we propose a *Perceptual consistency restoration* mechanism by minimizing the discrepancy between generated samples and input samples in both pixel and perceptual spaces. 2) To maintain the optimized latent vectors within the valid data manifold, we introduce a *Latent distribution consistency constraint* strategy to align generated samples with the clean data distribution. 3) We also apply a *Latent vector consistency prediction* scheme via an ensemble approach to enhance prediction reliability. CMAP fundamentally addresses adversarial perturbations at their source, providing a robust purification. Extensive experiments on CIFAR-10 and ImageNet-100 show that our CMAP significantly enhances robustness against strong adversarial attacks while preserving high natural accuracy.

Index Terms—Deep neural networks, Adversarial samples, Adversarial purification, Consistency models.

I. INTRODUCTION

DEEP neural networks (DNNs) have achieved remarkable success across various domains, including image classification [1], [2], natural language processing [3], [4] and speech

Shuhai Zhang, Jiahao Yang, and Mingkui Tan are with the School of Software Engineering, South China University of Technology, also with the Pazhou Laboratory, Guangzhou, China. E-mail: shuhaihangshz@gmail.com, yijiahao81@gmail.com, mingkuitan@scut.edu.cn.

Hui Luo is with the National Key Laboratory of Optical Field Manipulation Science and Technology, CAS, also with the Institute of Optics and Electronics, CAS, Chengdu, China. E-mail: luohui19@mails.ucas.ac.cn.

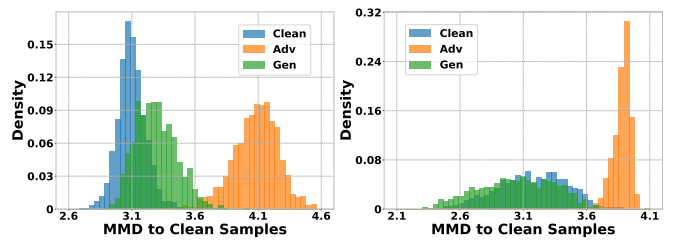
Jie Chen is with the School of Electronic and Computer Engineering, Peking University, Beijing 100871, China, and also with Peng Cheng Laboratory, Shenzhen 518066, China. E-mail: jiechen2019@pku.edu.cn

Li Wang is with the Department of Mathematics and the Department of Computer Science and Engineering, University of Texas at Arlington, Arlington, TX 76019 USA. E-mail: li.wang@uta.edu.

Feng Liu is with Computing and Information Systems, University of Melbourne. E-mail: fengliu.ml@gmail.com.

Bo Han is with Department of Computer Science, Hong Kong Baptist University. E-mail: bhanml@comp.hkbu.edu.hk.

* Authors contributed equally, † Corresponding author.



(a) CIFAR-10, consistency model [15] (b) ImageNet, diffusion model [16]

Fig. 1. Histograms of MMD distances [17] between the features of clean (Cln) and clean samples v.s. generated (Gen) and clean samples v.s. adversarial (Adv) samples and clean samples on CIFAR-10 and ImageNet. The results demonstrate that the generated samples are close to the clean ones but are far from the adversarial ones.

recognition [5], [6], and even in complex tasks like navigation planning [7]. However, DNNs are vulnerable to *adversarial samples* [8], [9], which are typically generated by introducing small and often imperceptible perturbations to inputs, causing the model to yield undesirable outputs [10]. These adversarial samples pose a significant threat to the deployment of DNNs in real-world scenarios, particularly in safety-critical applications, e.g., autonomous navigation systems [11], [12] and medical diagnosis [13], [14]. As DNNs become increasingly integrated into our lives, developing advanced adversarial defense methods becomes very urgent and imperative.

To improve the robustness of models against these threats, numerous adversarial defense strategies have been proposed [18]–[22]. Among them, *adversarial training* [18], [19], [23]–[25] stands out as a typical defense method, which involves augmenting the training data set with adversarial samples and then iteratively training the model with these augmented data, thereby enhancing its ability to defend these attacks. However, one significant drawback is the substantial computational cost of generating adversarial samples and incorporating them into the training process [26]. Moreover, adversarial training tends to be specific to some types of attacks during training, leaving the model vulnerable to unseen attacks [20], [21], [27], [28].

Another parallel route to improve robustness is *adversarial purification*, which preprocesses inputs to eliminate or neutralize adversarial perturbations with generative models before feeding them into the model [20], [21], [27], [28]. This process is independent of the model architecture or training, making it effective against various adversarial attacks compared with adversarial training, providing a versatile defense mechanism. However, it still suffers from mode collapse and low-quality sampling in generative models, which can lead to incomplete purification and the introduction of artifacts [21], [29], [30].

Recently, given the powerful capabilities of diffusion models in generating high-quality samples [16], [31]–[33], *diffusion-based adversarial purification* methods [20]–[22] have shown state-of-the-art defense performance. The diffusion model operates by a forward diffusion process that gradually adds noise to an input, followed by a reverse denoising process that removes this noise to recover the original data [31], [34]. A key advantage is its ability to purify noisy samples back to a clean distribution, incorporating randomness, which enhances its effectiveness as an adversarial purification tool [21], [22]. Given these merits, existing adversarial purification strategies [21], [22] add noise to adversarial samples at a specific diffusion timestep and recover the diffused samples through the reverse denoising. However, **two major challenges remain**: 1) *Incomplete removal of adversarial noise*: Adversarial noise often differs significantly from the noise added during the diffusion process, so even with denoising, only portions of the noise resembling the added noise can be removed, making it challenging to completely eliminate adversarial perturbations, especially on large-scale datasets [21], [22]. 2) *Inconsistent noise levels*: A specific diffusion timestep struggles to handle varying noise-level attacks, making it difficult to use a unified approach against diverse adversarial attacks [21], [22].

In this paper, we break away from traditional adversarial purification methods by focusing on the clean data *manifold*. Using generative models, we seek to identify latent vectors corresponding to the input samples on this manifold, thus fundamentally removing the potential adversarial perturbations from the data source. To this end, we reveal a crucial observation: **samples generated by a well-trained generative model are close to clean ones but far from adversarial ones**. As shown in Fig. 1, the MMD distances [17] between generated and clean sample features are *comparable* to those between clean samples, but are *significantly smaller* than those between adversarial and clean samples. This suggests that the latent space of the generative model aligns with the clean data manifold, enabling it to generate samples that resemble clean data and are far from adversarial perturbations. Based on this, we can optimize a latent vector within the latent space of the generative model to generate a sample as close to the original as possible, restoring the sample to the clean data manifold.

Unlike traditional diffusion-model-based adversarial purification methods [20]–[22], we employ a pre-trained consistency model [15], a diffusion model with deterministic generation and efficient one-step image synthesis, making it well-suited for this task. With the pre-trained consistency model, we propose a **Consistency Model-based Adversarial Purification (CMAP)** method, as illustrated in Fig. 2. During *optimization*, we introduce a **perceptual consistency restoration** mechanism, which optimizes latent vectors within the latent space of the pre-trained consistency model, projecting the input sample back onto the data manifold. To maintain these optimized latent vectors in the valid manifold and avoid overfitting to adversarial noise, we enforce a **latent distribution consistency constraint** strategy, ensuring alignment with the underlying distribution of clean data. For the final *prediction*, we employ a **latent vector consistency prediction** scheme to aggregate labels from multiple optimized latent vectors for each input,

leveraging their diversity to improve the stability and reliability of the overall outputs. By focusing on the clean data manifold and leveraging the latent space of a pre-trained consistency model, CMAP fundamentally addresses adversarial noise at its source. Unlike traditional defenses operating in the input space, our approach optimizes latent vectors that inherently align with the structure of clean data, effectively filtering out adversarial perturbations off the clean data manifold.

Specifically, the *perceptual consistency restoration* mechanism minimizes the mean absolute error (MAE [35]) while maximizing the structure similarity index measure (SSIM [36]) between the test input and the sample generated by the optimized latent vector. The rationale is that the adversarial samples typically reside close to the data manifold of clean examples in pixel space [37]–[39]. MAE focuses on correcting pixel-wise deviations, ensuring generated samples closely resemble the test sample. Meanwhile, SSIM restores perceptual and structural features [40], ensuring the recovered samples align with the manifold on pixel discrepancies while preserving the essential high-level features that define the data distribution. This dual optimization strategy leverages the manifold structure to achieve both pixel-level fidelity and perceptual integrity, resulting in semantically meaningful generated images.

The *latent distribution consistency constraint* strategy imposes a penalty on the optimized latent vectors during optimization using a mean squared error (MSE [41]) loss, which enforces a Gaussian distribution constraint across multiple sampled latent vectors for each test sample. This ensures that the latent vectors remain aligned with the *clean* data manifold, facilitating the generation of samples that reflect the clean data distribution. MSE is particularly effective here as it offers a straightforward and effective way to quantify distributional differences by focusing on means and variances, which are the key characteristics defining the manifold structure.

The *latent vector consistency prediction* scheme employs label voting across multiple optimized latent vectors for each test sample. This scheme ensures that the final prediction is robust and closely aligned with the underlying data manifold by fully utilizing the diversity of latent vectors for each sample. By aggregating predictions from multiple points on the manifold, it reduces the risk of outliers or deviations caused by adversarial perturbations. Similar multi-sampling defense mechanisms have been effectively used in prior works [20], [42].

Furthermore, we provide a consistency-disruption attack tailored to our CMAP. The attack results highlight the strong robustness of CMAP, suggesting that crafting adversarial samples within the latent space of a well-trained diffusion model is difficult, which aligns with the findings in Fig. 1. We also empirically compare our method with the latest adversarial training and purification methods against various strong attack benchmarks [22], [43]. Extensive experiments on CIFAR-10 and ImageNet-100 demonstrate the superior performance of our method. Notably, our CMAP shows absolute improvements of up to 18.73% \uparrow against PGD [18]+EOT [44] attacks and 8.27% \uparrow against AutoAttack [43] on CIFAR-10, and up to 6.47% \uparrow against PGD+EOT attacks on ImageNet-100 compared with SOTA methods, respectively, in robust accuracy.

We summarize our main contributions as follows:

- We reveal that samples generated by a well-trained generative model are near clean ones but far from adversarial ones. Leveraging this, we break away from traditional adversarial purification by focusing on the clean data manifold. We propose Consistency Model-based Adversarial Purification (CMAP), which optimizes latent vectors in the latent space of a consistency model to generate samples resembling the original, effectively restoring them to the clean data manifold.
- We introduce a perceptual consistency restoration mechanism to align generated samples with the data manifold at the pixel level while preserving high-level perceptual features. Additionally, we theoretically show that a distribution shift occurs between the latent vectors of clean and their adversarial samples, potentially introducing adversarial noise during restoration. To address this, we enforce a latent distribution consistency constraint strategy to maintain optimized latent vectors within the valid manifold, ensuring the samples are generated from the clean data distribution.
- We incorporate a latent vector consistency prediction scheme to enhance the stability and reliability of the final prediction. We also provide a consistency-disruption attack tailored to our CMAP. Experiments on CIFAR-10 and ImageNet-100 exhibit the superior performance of CMAP in robust and stand accuracy across various attacks. Notably, CMAP is agnostic to classifier architectures or attack types, using a unified defense operation, unlike prior adversarial purification that requires distinct hyperparameters for different attacks.

II. RELATED WORK

A. Diffusion Models and Consistency Model

Diffusion models have emerged as a potent family of probabilistic generative models, exhibiting outstanding performance across various applications [31], [34], [45], [46]. The key to all approaches in this family is to progressively perturb images to noise via Gaussian perturbations and then generate samples from noise via sequential denoising steps. The concept of the diffusion model originated from Sohl-Dickstein et al. [47]. Enlightened by non-equilibrium statistical physics, they use two learnable Markov chains to implement the perturbation and denoising process. Subsequently, Ho et al. [34] introduce Denoised Diffusion Probabilistic Model (DDPM) to reconstruct noise instead of image in the reverse Markov chain by training a U-Net network. Song et al. [31], [45] propose a similar strategy, called the Score-based Generative Model (SGM), which learns the score function of the intensifying noise sequence injected to images using deep neural networks, and leverages annealed Langevin dynamics to remove noise and generate samples. Immediately after that, DDPM and SGM are unified into the form of the score stochastic differential equation by Song et al. [46], extending the case to infinite time steps or noise levels, leading to the continuous-time diffusion model.

However, diffusion models are bottlenecked by their slow sampling speed due to the large number of evaluation steps. The Denoising Diffusion Implicit Model (DDIM) [48] extends the original DDPM to non-Markovian cases, enabling faster generation with fewer denoising steps. DPM-solver [49] exploits the semi-linear structure of probability flow ODE to

develop a more efficient ODE solver. Progressive Distillation [50] suggests distilling the full sampling process into a faster sampler parameterized as a neural network.

Inspired by the theory of the continuous-time diffusion model, the Consistency Model [15] supports single-step generation that obtains consistent images from arbitrary sampling points that belong to the same PF ODE trajectory, enforcing the proposed self-consistency property. Consistency models can be trained in either the distillation mode or the isolation mode. Moreover, it still allows iterative generation for zero-shot data editing and trade-offs between sample quality and computing.

B. Adversarial Attack

Numerous studies have been explored to attack deep models by introducing imperceptible perturbations into input data [18], [43], [51], [52]. Depending on the attacker's level of access to the model, adversarial attacks are categorized into white-box attacks and black-box attacks. White-box attackers have complete access to the target model's structure and parameters, enabling them to induce incorrect predictions directly through gradient ascent. In contrast, black-box attackers can only control the input and output of the target model, lacking internal details. They typically employ a proxy model to generate adversarial samples, which are then applied to the target.

The phenomenon of misleading classifiers with small perturbations in images is first discovered and demonstrated by Szegedy et al. [53]. Inspired by this, Goodfellow et al. [51] propose the Fast Gradient Sign Method (FGSM), which introduces a single-step perturbation along the gradient direction of the loss function to generate adversarial samples. Madry et al. [18] further provide an iterative implementation of FGSM called Projected Gradient Descent (PGD), which projects the perturbed sample in each iteration to maintain similarity with the original one. While these attacks adopt ℓ_∞ -norm or ℓ_2 -norm constraints, Papernot et al. [54] propose the Jacobian Saliency Map Attack (JSMA) to generate adversarial samples by constraining ℓ_0 -norm of the perturbation, with only a few pixel modifications required. Unlike traditional methods that seek a single perturbation, AutoAttack [43] conducts diverse and targeted attacks to explore different vulnerabilities of the model. Additionally, Backward Pass Differentiable Approximation (BPDA) [52] computes the gradient of the non-differentiable function using a differentiable approximation, which is often an effective attack for defense methods that rely on gradient obfuscation, particularly purification methods based on stochastic gradients of the diffusion process.

C. Adversarial Defense

In the realm of adversarial defenses, existing approaches are primarily categorized into two main strategies: adversarial training and adversarial purification.

Adversarial Training. Adversarial training [18], [19], [23]–[25] has emerged as one of the most effective defense mechanisms against adversarial examples by incorporating adversarial perturbations during the training process. Huang et al. [55] define this as a min-max optimization, aiming to minimize the worst-case classification error induced by

adversarial examples during training. Shaham et al. [56] further approach the min-max problem from the perspective of robust optimization and propose a comprehensive framework for adversarial training. Madry et al. [18] claim that iterative attacks with more refined perturbation directions facilitate more effective adversarial training. These PGD-based adversarial training method significantly improves robustness by employing PGD attack to approximate the inner maximizing loop. Building on this foundation, Zhang et al. [57] and Pang et al. [23] focus on improving the trade-off between robustness and accuracy. Zheng et al. [24] leverage the high transferability of models across different training epochs to enhance the efficiency and effectiveness of adversarial training.

Some data-augmentation techniques are introduced into the process of adversarial training. For instance, Jorge et al. [25] introduce noise around clean samples to reinforce single-step adversarial training and mitigate the risk of catastrophic overfitting. Goyal et al. [19] leverage samples generated by the generative model to offer more diverse augmentations, thereby improving the efficiency of adversarial training. However, these adversarial training methods often suffer from substantial performance degradation when facing attacks not encountered during training. Furthermore, the computational demands for training across various classifiers and attack types are exceptionally high. In contrast, our CMAP, being both attack-agnostic and classifier-agnostic, offers a more flexible “plug-and-play” solution without requiring extensive retraining.

Adversarial Purification. Adversarial purification through generative models is a preprocessing strategy designed to purify adversarial samples before classification. It typically involves training generative models to capture the underlying distribution of clean images, enabling the reconstruction of the clean versions from their adversarial counterparts. For example, Samangouei et al. [58] introduce Defense-GAN, leveraging the generative power of GANs to purify adversarial images. Song et al. [59] observe that adversarial images predominantly fall in low-probability regions of the training distribution and design PixelDefend, an autoregressive generative model, to purify adversarial images. Similarly, Srinivasan et al. [60] drive off-manifold adversarial samples towards high-density regions of the data generating distribution by the Metropolis adjusted Langevin algorithm (MALA) [61]. Moreover, studies such as [62]–[64] demonstrate that energy-based models (EBMs) are also effective for adversarial purification.

Benefiting from the superiority of the diffusion-based generative models, there’s a growing interest in their application for adversarial purification. Yoon et al. [20] achieve purification by gradually denoising the adversarial images, with the stopping threshold determined through score matching to avoid over-purification. DiffPure [21] adopt a different approach by first adding noise to adversarial samples and then restoring clean images via a reverse denoising process. Similarly, GDMP [37] facilitate the generation of clean samples by introducing guidance information into the reverse denoising phase. However, these methods continue to face challenges in balancing the incomplete removal of adversarial noise with the precise restoration of structural textures, as well as addressing the inconsistency in noise levels across different attack types.

III. PRELIMINARIES

A. Adversarial Attack

The typical goal of adversarial attack is to mislead the target classifier by crafting a sample with imperceptible perturbation [18], [57], whose general process can be formulated as:

Definition 1. (Adversarial Sample) Let $\mathcal{D} = \{(\mathbf{x}_i, y_i)\}_{i=1}^n$ denote a collection of \mathbf{x}_i from the input space $\mathcal{X} \subset \mathbb{R}^d$ and y_i as its ground-truth label defined in a label set $\mathcal{C} = \{1, \dots, C\}$, and \hat{h} be a well-trained classifier on \mathcal{D} . An adversarial sample $\hat{\mathbf{x}}$ regarding \mathbf{x} with perturbation ϵ is generated as:

$$\hat{\mathbf{x}} = \arg \max_{\tilde{\mathbf{x}} \in \mathcal{B}(\mathbf{x}, \epsilon)} \mathcal{L}(\hat{h}(\tilde{\mathbf{x}}), \mathbf{y}), \quad (1)$$

where $\mathcal{B}(\mathbf{x}, \epsilon) = \{\mathbf{x}' \in \mathcal{X} \mid d(\mathbf{x}, \mathbf{x}') \leq \epsilon\}$, d is some distance (e.g., ℓ_2 or ℓ_∞ distance), and \mathcal{L} is some loss function. For simplicity, we denote $\hat{\mathbf{x}} = \mathbf{x} + \epsilon_a$ as the adversarial sample with the adversarial perturbation ϵ_a .

B. Adversarial Purification

Adversarial purification aims to use a generative model to restore the clean sample from the adversarial sample [20]–[22], [65], which is defined as below.

Problem 1. (Adversarial Purification) Let $\mathcal{X} \subset \mathbb{R}^d$ be a separable metric space and p be a Borel probability measure on \mathcal{X} . Giving IID samples $\mathcal{D}_p = \{\mathbf{x}^{(i)}\}_{i=1}^n$ from the distribution p and a ground-truth labeling mapping $h : \mathbb{R}^d \rightarrow \mathcal{C}$ with $\mathcal{C} = \{1, \dots, C\}$ being a label set. Assuming that the attacker has access to some well-trained classifier \hat{h} and generates samples $\mathcal{D}' = \{\hat{\mathbf{x}}^{(i)}\}_{i=1}^m$ that mislead the classifier, we wish to restore samples $\hat{\mathbf{x}}_i$ in \mathcal{D}' back to the corresponding \mathbf{x}_i in \mathcal{D}_p .

C. Continuous-time Diffusion Models

Diffusion models, also referred to as score-based generative models [46], sequentially corrupt input data with slowly increasing noise, and then learn to reverse this corruption to form a generation process.

Given a data distribution $p(\mathbf{x})$, diffusion models initiate a forward diffusion process $\{\mathbf{x}_t\}_{t=0}^T$ indexed by continuous time $t \in [0, T]$, such that $\mathbf{x}_0 := \mathbf{x} \sim p(\mathbf{x})$ represents the data distribution, and $\mathbf{x}_T \sim p_T(\mathbf{x})$ is the prior distribution. This diffusion process can be modeled by a **stochastic differential equation (SDE)** with positive time increments:

$$d\mathbf{x} = \mathbf{f}(\mathbf{x}, t)dt + g(t)d\mathbf{w}, \quad (2)$$

where $\mathbf{f}(\cdot, t) : \mathbb{R}^d \rightarrow \mathbb{R}^d$ is a vector-valued function called drift coefficient, $g(\cdot) : \mathbb{R} \rightarrow \mathbb{R}$ is a scalar function called diffusion coefficient, and \mathbf{w} is a standard Wiener process.

Denote by $p_t(\mathbf{x})$ the marginal distribution of \mathbf{x}_t with $p_0(\mathbf{x}) := p(\mathbf{x})$. By starting from \mathbf{x}_T and reversing the diffusion process, wherein the reverse of a diffusion is also a diffusion [66], we can reconstruct samples $\mathbf{x}_0 \sim p_0(\mathbf{x})$. The reverse process is given by the reverse-time SDE:

$$d\mathbf{x} = [\mathbf{f}(\mathbf{x}, t) - g(t)^2 \nabla_{\mathbf{x}} \log p_t(\mathbf{x})]dt + g(t)d\bar{\mathbf{w}}, \quad (3)$$

where $\bar{\mathbf{w}}$ is a standard Wiener process when time flows backwards from T to 0, dt is an infinitesimal negative timestep.

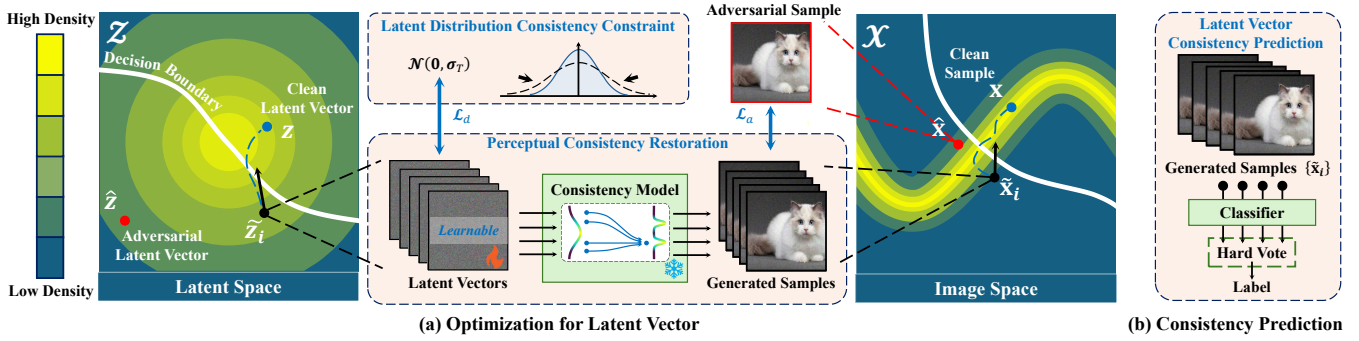


Fig. 2. Overview of the proposed CMAP. (a) Given a pre-trained consistency model, we optimize a set of latent vectors $\{\tilde{\mathbf{z}}_i\}$ within its latent space \mathcal{Z} to generate samples $\{\tilde{\mathbf{x}}_i\}$ as close to the original test sample $\tilde{\mathbf{x}}$ while removing potential adversarial perturbations by *perceptual consistency restoration* mechanism and *latent distribution consistency constrain* strategy, illustrated here for $\tilde{\mathbf{x}}$ as an adversarial sample. The perceptual consistency restoration mechanism employs \mathcal{L}_a consisting of MAE and SSIM loss to align generated samples with the clean data manifold, while the latent distribution consistency constrain strategy uses a Gaussian distribution constrain loss \mathcal{L}_d to ensure that the optimized vectors $\{\tilde{\mathbf{z}}_i\}$ stay within the valid manifold. (b) After optimization, we employ a *latent vector consistency prediction* scheme by a label voting across the final generated images to determine the final prediction for the test sample $\tilde{\mathbf{x}}$.

Given the inherent denoising ability and randomness of diffusion models, many studies [20]–[22] use them for adversarial purification by adding noise at a specific timestep to the test sample during the forward diffusion process via Eqn. (2) and gradually removing it through reverse denoising steps via Eqn. (3). However, if the noise level is too low, it fails to cover adversarial noise, resulting in poor defense performance; if too high, it significantly reduces natural accuracy. Additionally, different attacks require varying noise levels, making it difficult to defend diverse adversarial attacks [21], [22].

D. Consistency Model

The consistency model [15] is a new type of generative model that supports both single-step generation and multi-step generation for trade-offs between quality and computing. Its core design involves mapping each sampling point on an ODE-based diffusion trajectory to its origin by learning a consistency model $f_\theta : (\mathbf{x}_t, t) \mapsto \mathbf{x}_\delta$, where δ is a fixed positive number close to 0. Formally, the consistency model f_θ is required to satisfy the following self-consistency property:

$$f_\theta(\mathbf{x}_t, t) = f_\theta(\mathbf{x}_{t'}, t'), \forall t, t' \in [\delta, T]. \quad (4)$$

Following [15], to ensure that $f_\theta(\mathbf{x}_\delta, \delta) = \mathbf{x}$, the consistency model f_θ is parameterized as:

$$f_\theta(\mathbf{x}_t, t) = c_{\text{skip}}(t)\mathbf{x} + c_{\text{out}}(t)F_\theta(\mathbf{x}_t, t), \quad (5)$$

where $c_{\text{skip}}(t)$ and $c_{\text{out}}(t)$ are differentiable functions with $c_{\text{skip}}(\delta)=1$ and $c_{\text{out}}(\delta)=0$, and $F_\theta(\mathbf{x}_t, t)$ is a deep neural network. Throughout the paper, we omit the timestep T and use $f_\theta(\cdot)$ to denote the generated sample for simplicity.

A consistency model can be either distilled from a well-trained diffusion model or directly trained from scratch, known as consistency distillation and consistency training [15].

Consistency distillation enforces the self-consistency property by defining a consistency distillation loss as follows:

$$\mathcal{L}_{\text{CD}}(\theta, \theta^-; \phi) = \mathbb{E}_{\mathbf{x}, t} [d(f_\theta(\mathbf{x}_{t_{n+1}}, t_{n+1}), f_{\theta^-}(\hat{\mathbf{x}}_{t_n}^\phi, t_n))], \quad (6)$$

$$\hat{\mathbf{x}}_{t_n}^\phi = \mathbf{x}_{t_{n+1}} + (t_n - t_{n+1})\Phi(\mathbf{x}_{t_{n+1}}, t_{n+1}, \phi),$$

where θ^- is a target model updated via the exponential moving average (EMA) of the parameter θ , $\hat{\mathbf{x}}_{t_n}^\phi$ denotes a one-step

estimation of \mathbf{x}_{t_n} of $\mathbf{x}_{t_{n+1}}$ with Φ as the one-step ODE solver applied to PF ODE, and d is a distance between two samples. When using the Euler solver, we have $\Phi(\mathbf{x}, t, \phi) = -ts_\phi(\mathbf{x}, t)$, with $s_\phi(\mathbf{x}, t)$ refers to the score model.

Consistency training approximates the score function $\nabla_{\mathbf{x}} \log p_t(\mathbf{x})$ with the following unbiased estimator, therefore avoid the pre-trained score model $s_\phi(\mathbf{x}, t)$ altogether:

$$\nabla_{\mathbf{x}} \log p_t(\mathbf{x}) = -\mathbb{E} \left[\frac{\mathbf{x}_t - \mathbf{x}}{t^2} \mid \mathbf{x}_t \right], \quad (7)$$

and similar to consistency distillation, the consistency training loss is obtained as follows:

$$\mathcal{L}_{\text{CT}}(\theta, \theta^-) = \mathbb{E}_{\mathbf{x}, t} [d(f_\theta(\mathbf{x} + t_{n+1}\mathbf{z}, t_{n+1}), f_{\theta^-}(\mathbf{x} + t_n\mathbf{z}, t_n))], \quad (8)$$

where $\mathbf{z} \sim \mathcal{N}(\mathbf{0}, \mathbf{I})$. Moreover, it can be proven that $\mathcal{L}_{\text{CD}}(\theta, \theta^-; \phi) = \mathcal{L}_{\text{CT}}(\theta, \theta^-) + o(\Delta t)$.

Advantages of consistency models for adversarial purification: 1) *The ODE-based generation follows a deterministic trajectory.* Different from previous diffusion models [34], [46], which may generate different samples with a latent vector from an Gaussian distribution, the ODE-based consistency model generates a unique sample from a latent vector, ensuring a *deterministic* latent vector for each sample. This lays an important foundation for iterative optimization in finding the latent vector corresponding to a sample on the data manifold. 2) *The consistency model enables one-step generation.* Unlike other diffusion models [34], [46] that require multiple iterations to generate high-quality images, the consistency model can produce a reasonably good image in a single step, facilitating efficient iterative latent vector optimization.

IV. PROPOSED METHODS

Existing diffusion-based purification methods [20]–[22] inject Gaussian noise into the test sample and then recover them to purified samples through the denoising process. However, these methods suffer from incomplete removal of adversarial noise due to the inherent property of the diffusion and denoising processes, and inconsistent noise levels across different attacks. To address this, we aim to break away from this traditional paradigm by focusing on the clean data manifold.

Algorithm 1 Adversarial purification with CMAP.

Input: test sample $\hat{\mathbf{x}}$, consistency model f_θ , latent distribution $\mathcal{N}(\mathbf{0}, \sigma_T \mathbf{I})$, the number of sampling K , total optimization iterations T , step size η , classifier h .

Sample $\tilde{\mathbf{z}}^0 = \{\tilde{\mathbf{z}}_i\}_{i=1}^K \sim \mathcal{N}(\mathbf{0}, \sigma_T \mathbf{I})$.

for $j = 1, \dots, T$ **do**

 // *Perceptual consistency restoration.*

 Obtain the restoration loss $\mathcal{L}_a(\tilde{\mathbf{z}}^{j-1}, \hat{\mathbf{x}})$ using Eqn. (10).

 // *Latent distribution consistency constraint.*

 Obtain the latent distribution constrain loss $\mathcal{L}_d(\tilde{\mathbf{z}}^{j-1})$ using Eqn. (12).

 Update the latent vectors by gradient descent:

$$\tilde{\mathbf{z}}^j \leftarrow \tilde{\mathbf{z}}^{j-1} - \eta \cdot \frac{\partial [\mathcal{L}_a(\tilde{\mathbf{z}}^{j-1}, \hat{\mathbf{x}}) + \beta \mathcal{L}_d(\tilde{\mathbf{z}}^{j-1})]}{\partial \mathbf{z}_{j-1}}.$$

end for

 // *Latent vector consistency prediction.*

 Obtain the generated samples $\tilde{\mathbf{x}} \leftarrow f_\theta(\tilde{\mathbf{z}}^{T_{\text{def}}})$.

 Obtain the prediction \hat{y} via the label voting using Eqn. (14).

Output: \hat{y} .

Motivated by the observation that samples generated by a well-trained generative model are close to clean ones but distant from adversarial ones (see Fig. 1 and Sec. V-B), we aim to optimize latent vectors within the latent space of a generative model to generate samples to restore clean data. Leveraging the consistency model with deterministic generation and efficient one-step image synthesis, we propose **Consistency Model-based Adversarial Purification** (CMAP). Particularly, we introduce a *perceptual consistency restoration* mechanism to optimize latent vectors to align generated samples with the data manifold (Sec. IV-A), a *latent distribution consistency constraint* strategy to maintain the optimized vectors within the valid manifold (Sec. IV-B), and a *latent vector consistency prediction* scheme to stabilize the final output by aggregating the results of the multiple optimized vectors (Sec. IV-C). The framework of CMAP is illustrated in Fig. 2, with its algorithm in Alg. 1. Last, we provide a consistency-disruption attack tailored to CMAP in Sec. IV-D and its algorithm in Alg. 2.

Given a test sample $\hat{\mathbf{x}}$, the overall optimization for latent vectors $\tilde{\mathbf{z}} = \{\tilde{\mathbf{z}}_i\}_{i=1}^K$ in our CMAP is formulated as:

$$\min_{\tilde{\mathbf{z}}} \mathcal{L}_a(\tilde{\mathbf{z}}, \hat{\mathbf{x}}) + \beta \mathcal{L}_d(\tilde{\mathbf{z}}), \quad (9)$$

where \mathcal{L}_a is the perceptual consistency restoration loss defined in Eqn. (10), \mathcal{L}_d is the latent distribution consistency constraint in Eqn. (12), and β is a hyper-parameter.

A. Perceptual Consistency Restoration

Previous adversarial purification methods [20]–[22] typically restore the original data by directly modifying the test sample. However, this approach inherently struggles to fully eliminate adversarial perturbations, as it addresses the processed data rather than targeting the underlying causes of the perturbation. To address this, we propose a *perceptual consistency restoration* mechanism focusing on the clean data manifold, which optimizes latent vectors within a generative model’s latent space to generate samples resembling the test sample, thus removing potential adversarial perturbations at their source.

One straightforward approach to achieve the above goal is to optimize GAN latent vectors, which, however, often produces semantically unclear or structurally blurred images (see Fig. 8 in Appendix), leading to inferior defense performance shown in [21]. A possible reason is that the latent space, constrained by a low-dimensional normal distribution, limits its capacity for representation and semantic disentanglement [67], [68]. To overcome this, benefiting from the high-quality samples generated by editing latent vectors in diffusion models [32], [69]–[71], we can exploit a diffusion model to obtain an optimized latent vector. Unfortunately, one obvious limitation of diffusion models is their reliance on multi-step iterative processes to generate a single image, making them less suitable here. To circumvent this issue, we turn to consistency models [15], which offer the advantages of deterministic generation and efficient one-step image synthesis (see more details in Sec. III-D), making it well-suited for this task.

Formally, given a pre-trained consistency model f_θ , we sample a set of latent vectors $\{\tilde{\mathbf{z}}_i\}_{i=1}^K \sim \mathcal{N}(\mathbf{0}, \sigma_T \mathbf{I})$ from its latent distribution. We employ multiple latent vectors for two reasons: 1) Multiple latent vectors reduce the risk of selecting an outlier deviating too far from the Gaussian distribution center, ensuring more reliable optimization results; 2) Multiple latent vectors provide a basis for imposing constraints on the distribution of latent vectors during optimization (see Sec. IV-B). To restore the test sample, intuited that the adversarial samples typically reside near the manifold of clean data in the pixel space [37]–[39], we employ Mean Absolute Error (MAE [35]) and Structure Similarity Index Measure (SSIM [36]) to align the samples generated by the optimized latent vectors with the test sample, which is formulated as

$$\mathcal{L}_a(\tilde{\mathbf{z}}, \hat{\mathbf{x}}) = \frac{1}{K} \sum_{i=1}^K \|f_\theta(\tilde{\mathbf{z}}_i) - \hat{\mathbf{x}}\|_1 - \alpha \cdot \text{SSIM}(f_\theta(\tilde{\mathbf{z}}_i), \hat{\mathbf{x}}). \quad (10)$$

Here, we omit the time T in $f_\theta(\cdot)$ for simplicity. MAE focuses on preserving overall color and brightness, ensuring the sample aligns with the original test sample’s appearance on the manifold. Meanwhile, SSIM captures high-frequency textures and structural details, critical for representing the local structure of the manifold. Furthermore, our experiments show that SSIM aids in faster convergence, enabling the model to rapidly achieve a high-quality restoration that represents both pixel-level and perceptual consistency with the original sample.

Remark 1. *Note that traditional white-box attacks [18], [43], [51] typically rely on manipulating the leaf nodes of the computational graph to generate adversarial samples that can bypass purification methods. However, in our approach, we employ the Gaussian vector to generate samples, treating them as non-leaf nodes in the optimization process. This makes it difficult for gradient-based white-box attacks to effectively target our defense module, as adversarial perturbations cannot directly influence the latent space optimization.*

B. Latent Distribution Consistency Constraint

The perceptual consistency restoration mechanism can achieve moderate performance in both robust accuracy and

clean accuracy. However, it heavily depends on selecting an appropriate number of optimization iterations (see Fig. 3). Excessive iterations may cause the latent vector to fit the adversarial noises embedded in the input sample, making the generated sample increasingly similar to the adversarial input at the pixel level, until they become exactly same. This issue occurs because the optimization may unintentionally steer the latent vector away from the clean data manifold when aligning with the adversarial input [72]. To further clarify this, we derive the following theorem to provide insight into the distribution discrepancy between the latent vectors of clean and adversarial samples when the natural data follow a Gaussian distribution.

Theorem 1. *Assuming that the distribution of natural data $p(\mathbf{x}) = \mathcal{N}(\boldsymbol{\mu}_x, \sigma_x^2 \mathbf{I})$, where \mathbf{I} is an identity matrix, given a PF ODE sampling $d\mathbf{x} = -t\nabla_{\mathbf{x}} \log p_t(\mathbf{x})$ with $\mathbf{f}(\mathbf{x}, t) = \mathbf{0}$ and $g(t) = \sqrt{2t}$, then for $\forall \mathbf{x} \in p(\mathbf{x})$ and its adversarial sample $\hat{\mathbf{x}} = \mathbf{x} + \epsilon_a$, we have*

$$\mathbf{x}_T - \hat{\mathbf{x}}_T \sim \mathcal{N}(\mathbf{0}, 2\sigma_{cl}^2 \mathbf{I}) + \boldsymbol{\mu}_\epsilon, \quad (11)$$

where $\boldsymbol{\mu}_\epsilon = \left(\mathbb{E}_t \frac{t}{\sigma_x^2 + t^2} - 1 \right) \epsilon_a$ and $\sigma_{cl}^2 = \mathbb{E}_t \frac{t^2}{\sigma_x^2 + t^2}$.

Proof. The proof is provided in Appendix VII.1. \square

Theorem 1 indicates that when tracing the ODE trajectory to find the corresponding latent vector for an adversarial sample, a significant distribution shift occurs between this latent vector and that of the original clean sample due to the term $\boldsymbol{\mu}_\epsilon$. Although the mean term can theoretically be zero (see Appendix VII.1), this scenario is highly unlikely in practical applications, where natural data distributions are typically diverse. Consequently, it is essential to ensure that the optimized latent vectors remain within a valid and meaningful region of the latent space, thereby maintaining the alignment of the restored image with the clean distribution and avoiding overfitting adversarial perturbations.

To achieve the above goal, we propose a *latent distribution consistency constraint* strategy to enforce the optimized latent vectors to stay close to the latent distribution of the pre-trained consistency model. Constraining a single sample to belong to a specific distribution may be a challenging task. Fortunately, the perceptual consistency restoration mechanism depicted in Sec. IV-A has already provided multiple optimized latent vectors corresponding to a single test input, which enables various techniques of the distribution alignment on the optimized vectors, such as Wasserstein distance [73] and maximum mean discrepancy [17], [74].

In this work, we employ an MSE loss to align the mean and variance of the multiple optimized latent vectors with the latent distribution of the consistency model since it has been widely used as a metric to assess distribution alignment [75], [76]. Formally, the latent distribution consistency constraint loss is provided as follows:

$$\mathcal{L}_d(\tilde{\mathbf{z}}) = \|\mu(\{\tilde{\mathbf{z}}_i\}) - \mu_z\|_2^2 + \|\sigma(\{\tilde{\mathbf{z}}_i\}) - \sigma_z\|_2^2, \quad (12)$$

where $\mu(\{\tilde{\mathbf{z}}_i\}) = \frac{1}{K} \sum_{i=1}^K \tilde{\mathbf{z}}_i$, $\sigma^2(\{\tilde{\mathbf{z}}_i\}) = \frac{1}{K} \sum_{i=1}^K (\tilde{\mathbf{z}}_i - \mu(\{\tilde{\mathbf{z}}_i\}))^2$ are the empirical mean and variance of the optimized vectors, respectively, $\mu_z = \mathbf{0}$, $\sigma_z^2 = \sigma_T \mathbf{I}$ are the mean and variance of the latent distribution w.r.t the pre-trained consistency model.

MSE is computationally straightforward and can be particularly effective here. It directly aligns the first and second moments (e.g., mean and variance) of the latent vectors with the latent distribution. This approach effectively constrains the optimized latent vectors to maintain a statistical consistency to the latent distribution, preserving the underlying structure of the clean data manifold. Other techniques of the distribution alignment can be explored in future work. This strategy helps maintain the alignment of the generated samples with the clean data, effectively preventing the optimized latent vectors from drifting toward adversarial artifacts.

Thus far, we have detailed the optimization process in our CMAP. In fact, optimizing the objective function in Eqn. (9) implicitly minimizes an upper bound on the reconstruction loss for the *clean* sample, as shown in the following proposition.

Proposition 1. *Given a test sample $\hat{\mathbf{x}}$, it holds that optimizing a set of latent vectors $\{\tilde{\mathbf{z}}_i\}_{i=1}^K$ by Eqn. (9) gives an upper bound on the reconstruction for the clean sample \mathbf{x} :*

$$\frac{1}{K} \sum_{i=1}^K \|f_\theta(\tilde{\mathbf{z}}_i) - \mathbf{x}\|_1 + \beta \mathcal{L}_d(\tilde{\mathbf{z}}) \leq C + \mathcal{L}_a(\tilde{\mathbf{z}}, \hat{\mathbf{x}}) + \beta \mathcal{L}_d(\tilde{\mathbf{z}}), \quad (13)$$

where C is a constant related to the adversarial perturbation.

Proof. The proof is provided in Appendix VII.2. \square

The conclusion in Proposition (1) is evident. When the test sample $\hat{\mathbf{x}}$ is clean, minimizing $\mathcal{L}_a(\tilde{\mathbf{z}}, \hat{\mathbf{x}}) + \beta \mathcal{L}_d(\tilde{\mathbf{z}})$ directly reduces the loss between the generated and original clean samples; when $\hat{\mathbf{x}}$ is adversarial, this objective effectively tightens the upper bound on the reconstruction loss of the original clean sample. This suggests that our CMAP method not only aims to restore the clean data but also constrains adversarial perturbations, preventing significant reconstruction errors associated with the clean sample. The latent distribution consistency term $\mathcal{L}_d(\tilde{\mathbf{z}})$ further aligns the optimized latent vectors with the expected clean distribution, thereby reducing the likelihood of the reconstruction process yielding adversarial outputs. Consequently, the overall objective provides a strong regularization effect, pushing the optimization towards regions consistent with clean data, thus ensuring a smaller gap between the reconstructed sample and the original clean sample.

C. Latent Vector Consistency Prediction

While the perceptual consistency restoration mechanism and latent distribution consistency constraint strategy ensure that the generated samples are aligned with the clean data manifold and remain within a meaningful region of the latent space, there is still the potential for variability among the multiple optimized latent vectors. This variability can introduce inconsistencies in the generated samples, which may lead to fluctuations in the final classification results. To address this, we introduce the *latent vector consistency prediction* scheme to stabilize the output and enhance the robustness of our purification method.

In this scheme, we aggregate the predictions from multiple generated samples to produce a more reliable classification. Specifically, given a set of optimized latent vectors $\{\tilde{\mathbf{z}}_i\}_{i=1}^K$, we generate corresponding samples $\{\tilde{\mathbf{x}}_i\}_{i=1}^K$ with $\tilde{\mathbf{x}}_i = f_\theta(\tilde{\mathbf{z}}_i)$ and

Algorithm 2 Consistency-Disruption Attack against CMAP.

Input: clean sample \mathbf{x} and its label y , consistency model $f_\theta(\cdot)$, the number of alignment iterations T_{def} , the number of attack iterations T_{adv} , attack intensity ϵ , adversarial factor λ , attack step size η' , classifier \hat{h} .
 Obtain initialized latent vectors $\tilde{\mathbf{z}}^{T_{\text{def}}}$ via Alg. 1.
for $j = T_{\text{def}} + 1, \dots, T_{\text{def}} + T_{\text{adv}}$ **do**
 Obtain the generated samples $\mathbf{x}^{j-1} \leftarrow f_\theta(\tilde{\mathbf{z}}^{j-1})$.
 Project the samples into $\mathcal{B}(\mathbf{x}, \epsilon)$:
 $\mathbf{x}_{\text{adv}} \leftarrow \text{Proj}_{\mathcal{B}(\mathbf{x}, \epsilon)}(\mathbf{x}^{j-1})$.
 Update the latent vectors by gradient descent:
 $\tilde{\mathbf{z}}^j \leftarrow \tilde{\mathbf{z}}^{j-1} - \eta' \cdot \frac{\partial [\mathcal{L}_a(\tilde{\mathbf{z}}^{j-1}, \hat{\mathbf{x}}) + \beta \mathcal{L}_d(\tilde{\mathbf{z}}^{j-1}) - \lambda \cdot \mathcal{L}_{CE}(\mathbf{x}_{\text{adv}}, y)]}{\partial \mathbf{z}_{j-1}}$.
end for
 Obtain the adversarial samples $\mathbf{x}_{\text{adv}} \leftarrow f_\theta(\tilde{\mathbf{z}}^{T_{\text{def}}+T_{\text{adv}}})$.
 Project the samples into $\mathcal{B}(\mathbf{x}, \epsilon)$: $\mathbf{x}_{\text{adv}} \leftarrow \text{Proj}_{\mathcal{B}(\mathbf{x}, \epsilon)}(\mathbf{x}_{\text{adv}})$.
Output: \mathbf{x}_{adv} .

obtain their predicted labels $\{\hat{h}(\tilde{\mathbf{x}}_i)\}_{i=1}^K$ using the pre-trained classifier \hat{h} . The final prediction \hat{y} is then determined by a label voting mechanism, which selects the label with the highest vote count across all predictions:

$$\hat{y} = \arg \max_y \sum_{i=1}^K \mathbb{I} \left[\hat{h}(f_\theta(\tilde{\mathbf{x}}_i)) = y \right], \quad (14)$$

where $\mathbb{I}[\cdot]$ is an indicator function that returns 1 if the condition is true and 0 otherwise.

This label voting mechanism effectively reduces the impact of any individual outlier prediction, thereby stabilizing the overall decision-making process. By aggregating predictions from multiple latent vectors, the method leverages the collective information from diverse perspectives within the latent space, leading to a more consistent and robust final output.

Advantages of CMAP for adversarial purification: 1) *Shifted attack space:* Traditional adversarial attacks focus on generating perturbations in the input space, but our method operates in the latent space of a generative model. This *shift* forces attackers to generate perturbations in the latent space, which is unfamiliar and challenging for them to exploit effectively, thereby complicating the attack process. 2) *Latent distribution regularization:* Our method enforces regularization on the latent vectors, keeping them near a Gaussian distribution centered on clean data. This safeguard makes it difficult for adversarial perturbations to push the generated samples away from the clean data manifold. 3) *Stability of multiple samplings:* Our approach introduces diversity in the generated outputs by sampling multiple latent vectors. This further increases robustness because the attacker would need to successfully perturb all sampled latent vectors simultaneously to achieve a consistent attack, significantly raising the difficulty.

D. Consistency-Disruption Attack against CMAP

Given that traditional white-box attacks [18], [43], [51] are ineffective against our method, we recognize the importance of an attack strategy specifically tailored to our defense mechanism to rigorously evaluate the robustness of our CMAP. This attack

should be aware of the defense mechanism and seek to exploit any potential vulnerabilities. Under such circumstances, unlike traditional attacks that optimize perturbations in the input space, we propose a *consistency-disruption attack*, which navigates the latent space of a generative model to optimize the latent vectors during the purification process, steering generated samples away from the clean data manifold and toward adversarial regions.

To achieve the above goal, we modify the objective function in Eqn. (9) of our defense method by introducing an additional term that maximizes the cross-entropy loss between the prediction of the classifier and the true label of the sample. This attack can be formulated as follows:

$$\begin{aligned} \min_{\tilde{\mathbf{z}}} \mathcal{L}_a(\tilde{\mathbf{z}}, \mathbf{x}) + \beta \mathcal{L}_d(\tilde{\mathbf{z}}) - \lambda \mathcal{L}_{CE}(\mathbf{x}_{\text{adv}}, y), \quad (15) \\ \text{s.t., } \mathbf{x}_{\text{adv}} = \text{Proj}_{\mathcal{B}(\mathbf{x}, \epsilon)}(f_\theta(\tilde{\mathbf{z}})), \end{aligned}$$

where \mathcal{L}_{CE} is the cross-entropy loss, $\text{Proj}_{\mathcal{B}(\mathbf{x}, \epsilon)}(\cdot)$ projects the adversarial sample into a norm-ball. The hyper-parameter λ controls the strength of the adversarial attack.

To efficiently optimize the attack objection in Eqn. (15), we initialize the latent vectors $\tilde{\mathbf{z}}$ by leveraging our defense mechanism (without the loss term \mathcal{L}_{CE}) to find the optimized latent vectors corresponding to the clean sample. Starting from this initialization helps in maintaining closer proximity to the clean data manifold and then gradually introducing adversarial perturbations in the latent space by adding additional \mathcal{L}_{CE} loss. We provide a detailed attack procedure in Alg. 2. Note that this attack strategy can generate multiple adversarial samples corresponding to a single clean sample. The attack is considered successful if any of these samples manage to bypass the defense mechanism and lead to misclassification.

Our experiments in Sec. V-E demonstrate that while this attack poses a significant challenge to defense, our CMAP still exhibits strong robustness primarily due to our latent distribution consistency constraint strategy and the latent vector consistency prediction scheme, which jointly maintain the alignment of the purified samples with the clean distribution, highlighting the robustness and adaptability of our approach in adversarial settings. This attack provides a rigorous test of CMAP’s robustness, ensuring that our defense mechanisms are not easily bypassed by consistency-disruption strategies.

V. EXPERIMENTS

A. Experimental Settings

Datasets and network architectures. We conduct the experiments on two datasets: CIFAR-10¹ [81] and ImageNet² [82]. For ImageNet, we adopt its sub-dataset³, ImageNet-100, which includes 100 classes of the original 1000. This choice balances computational feasibility and dataset complexity, as training consistency models on larger datasets like ImageNet-1K is resource-intensive [15]. Notably, our method remains applicable on larger datasets if pre-trained consistency models are available. We use pretrained WideResNet [83] models of varying sizes for CIFAR-10 classification and ResNet [1] for

¹<https://www.tensorflow.org/datasets/catalog/cifar10>

²<https://image-net.org>

³<https://www.kaggle.com/datasets/ambityga/imagenet100>

TABLE I

STANDARD AND ROBUST ACCURACY AGAINST PGD+EOT AND AUTOATTACK WITH ℓ_∞ -NORM ($\epsilon = 8/255$) AND ℓ_2 -NORM ($\epsilon = 0.5$) ON CIFAR-10. ADVERSARIAL TRAINING (AT) AND ADVERSARIAL PURIFICATION (AP) STRATEGIES ARE EVALUATED. (* MODEL IS TRAINED WITH EXTRA DATA.)

Strategy		Method	Standard	PGD+EOT	AutoAttack	Strategy		Method	Standard	PGD- ℓ_2 +EOT	AutoAttack- ℓ_2			
WRN-28-10	AT	Gowal et al. [19]	87.51	<u>66.01</u>	63.38	WRN-28-10	AT	Rebuffi et al. [78] *	<u>91.79</u>	<u>85.05</u>	78.80			
		Gowal et al. [77] *	88.54	65.93	62.76			WRN-28-10	AT	Augustin et al. [79]	93.96	86.14	78.79	
		Pang et al. [23]	88.62	64.95	61.04					WRN-28-10	AT	Schwag et al. [80]	90.93	83.75
	AP	ADP [20]	85.66 \pm 0.51	33.48 \pm 0.86	59.53 \pm 0.87		WRN-28-10					AP	ADP [20]	85.66 \pm 0.51
		DiffPure [21]	<u>90.27\pm0.81</u>	48.27 \pm 1.86	64.93 \pm 2.14			WRN-28-10	AP				DiffPure [21]	90.27 \pm 0.81
		GNSP [22]	90.40\pm1.40	55.87 \pm 0.50	<u>70.40\pm1.80</u>					WRN-28-10	AP		GNSP [22]	90.40 \pm 1.40
CMAP (Ours)	88.73 \pm 0.50	74.60\pm1.59	78.67\pm1.90	WRN-28-10	AP	CMAP (Ours)	88.73 \pm 0.50					84.00 \pm 1.71	<u>83.40\pm1.44</u>	
WRN-70-16	AT	Rebuffi et al. [78] *	92.22			<u>69.97</u>	66.56	WRN-70-16	AT			Rebuffi et al. [78] *	95.74	89.62
		Gowal et al. [19]	88.75			69.03	66.10			WRN-70-16	AT	Gowal et al. [77] *	<u>94.74</u>	<u>88.18</u>
		Gowal et al. [77] *	<u>91.10</u>	68.66	65.87	WRN-70-16	AT					Rebuffi et al. [78]	92.41	86.24
	AP	ADP [20]	86.76 \pm 1.15	37.11 \pm 1.35	37.11 \pm 1.35				WRN-70-16			AP	ADP [20]	86.76 \pm 1.15
		DiffPure [21]	90.00 \pm 0.87	50.93 \pm 1.30	63.87 \pm 1.86					WRN-70-16	AP		DiffPure [21]	90.00 \pm 0.87
		GNSP [22]	90.53 \pm 0.58	56.07 \pm 0.83	<u>71.67\pm0.64</u>	WRN-70-16	AP						GNSP [22]	90.53 \pm 0.58
CMAP (Ours)	88.27 \pm 0.50	74.80\pm1.56	81.33\pm0.31	WRN-70-16	AP			CMAP (Ours)	88.27 \pm 0.50			82.93 \pm 1.45	<u>83.47\pm0.46</u>	

ImageNet-100. Particularly, we fine-tune the fully connected (FC) layer of classifiers to align predictions with the label space of ImageNet-100. By employing the automatic mixup [84], the classification accuracies are 78.62% for ResNet50, 78.08% for ResNet101 and 80.34% for WRN-50-2.

Implementation details. For the consistency models in our CMAP, we adopt the pretrained model released from the paper [15] on CIFAR-10, with only a conversion from the JAX implementation⁴ to the PyTorch version. While on ImageNet-100, we train the consistency model according to the consistency training following [15]. The diffusion trajectory of the consistency model aligns with that of the corresponding diffusion model [85], characterized by the parameters $\mu_T = 0$, $\sigma_0 = 0.002$ and $\sigma_T = 80$. Through the optimization parameters in our CMAP, we set $\alpha = 2$, $\beta = 5 \times 10^{-4}$ with 200 iterations on CIFAR-10 and $\alpha = 5 \times 10^{-3}$, $\beta = 1 \times 10^{-4}$ with 300 iterations on ImageNet-100.

Attacks methods. Following [22], we consider the commonly used ℓ_∞ and ℓ_2 white-box attack methods to evaluate our method, including PGD [18], AutoAttack [43] and BPDA [52]. To strengthen these attacks, we approximate the surrogate gradient by simulating the entire denoising process from the midpoint of the diffusion, as done in [22]. This approach substantially increases the effectiveness of attack, providing a more rigorous robustness evaluation of the defense methods. Specifically, we use 200 iterations for PGD and BPDA, while using the standard version of AutoAttack. Due to the stochasticity introduced by the randomized defenses, we also employ Expectation over Transformation (EOT) [44] with $n_{EOT} = 20$ when applying these attacks. For ℓ_∞ -norm attacks, we set to $\epsilon = 8/255$ on CIFAR-10 and $\epsilon = 4/255$ on ImageNet-100, and for ℓ_2 -norm attacks, we use $\epsilon = 0.5$. To further demonstrate the superiority of our method, we also consider the relatively high attack intensities on CIFAR-10, i.e., ℓ_∞ -norm with $\epsilon = 16/255$ and ℓ_2 -norm with $\epsilon = 1$.

Note that although existing strong white attacks such as AutoAttack, which are designed for direct perturbation in

TABLE II

STANDARD AND ROBUST ACCURACY AGAINST PGD+EOT ATTACK WITH ℓ_∞ -NORM ($\epsilon = 4/255$) AND ℓ_2 -NORM ($\epsilon = 0.5$) ON IMAGENET-100.

Classifier	Method	Standard	PGD+EOT	PGD- ℓ_2 +EOT
ResNet50	DiffPure [21]	58.40 \pm 1.10	28.57 \pm 1.82	46.96 \pm 1.44
	GNSP [22]	59.92 \pm 1.24	33.40 \pm 1.44	51.06 \pm 1.74
	CMAP (Ours)	61.93\pm1.86	39.87\pm2.58	54.67\pm1.40
ResNet101	DiffPure [21]	58.93 \pm 2.15	28.97 \pm 1.77	50.26 \pm 2.98
	GNSP [22]	60.38 \pm 2.89	32.61 \pm 1.39	51.98 \pm 2.15
	CMAP (Ours)	61.53\pm1.45	39.27\pm1.79	52.60\pm3.47
WRN-50-2	DiffPure [21]	61.44 \pm 1.02	28.57 \pm 2.41	51.46 \pm 1.35
	GNSP [22]	62.10 \pm 1.21	31.68 \pm 0.12	50.99 \pm 2.10
	CMAP (Ours)	63.33\pm2.32	40.47\pm3.59	54.73\pm3.18

the input space, may do not fully exploit the unique nature of our approach, applying them to our method ensures we are benchmarking against the most challenging and widely accepted adversarial settings. To this end, similar to attacking other diffusion-based adversarial purification methods [20]–[22], we select a timestep $t_{diff} = 0.3$ for attack based on the attack success rate (ASR) on both the classifier and purification module, as shown in Tab. V, with other settings kept the same. Moreover, we also provide a consistency-disruption attack tailored to our CMAP in Sec. IV-D to evaluate its robustness in Sec. V-E. We leave more white-box attacks specifically targeting generative-model-based purification frameworks like ours as an important direction for future work.

Baselines. To evaluate the effectiveness of our method, we compare with the state-of-the-art defense methods as reported in the standard benchmark RobustBench [86], including **adversarial training** [19], [23], [77]–[80] and **adversarial purification** [20]–[22]. Following the settings in [22], we inherit the results of the adversarial training methods from [22] due to the huge computational cost. For adversarial purification methods, DiffPure [21] uses diffusion timesteps of $t_{diff} = 0.1$ for the ℓ_∞ -norm and $t_{diff} = 0.075$ for the ℓ_2 -norm on CIFAR-10, and $t_{diff} = 0.15$ on ImageNet-100, respectively. GNSP [22] conducts purification in eight steps with $t_{diff} \in \{0.03 \times 4, 0.05 \times 2, 0.125 \times 2\}$ and $t_{diff} \in \{0.03 \times 4, 0.05 \times 2, 0.2 \times 2\}$ for both datasets.

⁴https://openai-public.blob.core.windows.net/consistency/jcm_checkpoints/cd-lpips/checkpoints/checkpoint_80

TABLE III

STANDARD AND ROBUST ACCURACY AGAINST BPDA+EOT ATTACK WITH ℓ_∞ -NORM ON CIFAR-10 ($\epsilon = 8/255$) AND IMAGENET-100 ($\epsilon = 4/255$). WIDERESNET-28-10 IS USED AS CLASSIFIER ON CIFAR-10 WHILE RESNET50 IS USED ON IMAGENET-100.

Dataset	Method	Standard	BPDA+EOT
CIFAR-10	ADP [20]	85.66 \pm 0.51	66.91 \pm 1.75
	DiffPure [21]	90.27 \pm 0.81	82.33 \pm 0.42
	GNSP [22]	90.40 \pm 1.40	88.53\pm1.14
	CMAP (Ours)	88.73 \pm 0.50	83.53\pm1.80
ImageNet-100	DiffPure [21]	58.40 \pm 1.10	46.56 \pm 2.12
	GNSP [22]	59.92 \pm 1.24	48.68 \pm 1.71
	CMAP (Ours)	61.93\pm1.86	49.47\pm2.12

TABLE IV

STANDARD AND ROBUST ACCURACY AGAINST ℓ_∞ -NORM ($\epsilon = 8/255$) AND ℓ_2 -NORM ($\epsilon = 0.5$) ATTACKS ON CIFAR-10, WITH WIDERESNET-28-10 USED AS CLASSIFIER.

Method	Standard	PGD- ℓ_2 +EOT	AutoAttack- ℓ_2	BPDA+EOT
DiffPure [21]	90.27 \pm 0.81	82.00 \pm 0.72	83.40 \pm 0.20	82.33 \pm 0.42
GNSP [22]	90.40 \pm 1.40	84.80\pm1.59	87.47 \pm 0.70	88.53 \pm 1.14
CMAP	88.73 \pm 0.50	84.00 \pm 1.71	83.40 \pm 1.44	83.53 \pm 1.80
CMAP+DiffPure [21]	91.33\pm0.23	83.60 \pm 0.69	88.47\pm0.31	89.47\pm0.23

Evaluation metrics. We consider two metrics to evaluate the performance of defense approaches: **standard accuracy** and **robust accuracy**. The standard accuracy assesses the classification performance of the defense model on clean samples, while the robust accuracy evaluates the model’s performance against adversarial attacks. An ideal purification module is supposed to enhance robust accuracy and strive to maintain standard accuracy. Considering the computational expense of applying several attacks and purification methods, especially on ImageNet-100, following [87], we randomly select a subset containing 500 samples and compute accuracy over it unless otherwise specified. Additionally, to ensure more stable and reliable results, we report the mean and standard deviation over 3 independent runs.

B. Observations on Generated Samples

We start by exploring the distributional characteristics of clean, adversarial and generated samples, which inspires the proposal of our CMAP. Leveraging its effectiveness in quantifying the distributional discrepancy between two distributions, we calculate the Expected Perturbation Score (EPS, $\mathbb{E}_{t \sim U(0,T)} \nabla_{\mathbf{x}} \log p_t(\mathbf{x})$) [88] that introduces increasing Gaussian noise to the sample and averages their scores, thereby extracting comprehensive distribution information from its multi-view observations. For generated samples, we employ multiple generative models [15], [16], [89] on both CIFAR-10 and ImageNet, while clean samples are randomly drawn from the corresponding datasets. For adversarial samples, we craft them by PGD- ℓ_∞ +EOT attack ($\epsilon = 4/255$). Taking 500 clean samples as a reference set, we compute the Maximum Mean Discrepancy (MMD) [17] between this set and each of the 500 clean (distinct from the reference), adversarial, generated samples. The results are then visualized through histograms.

TABLE V

ATTACK SUCCESS RATE (ASR) WITH SURROGATE GRADIENTS APPROXIMATED AT DIFFERENT DIFFUSION MIDPOINTS (t_{diff}). WE SELECT $t_{diff} = 0.3$ TO BALANCE THE ASR ON BOTH THE CLASSIFIER (CLF) AND THE PURIFICATION (PUR).

Attack	ASR	t_{diff}					
		0.1	0.2	0.3	0.4	0.5	
CIFAR-10	PGD+EOT	Clf	100.00%	99.20%	94.40%	28.80%	5.40%
		Pur+Clf	16.00%	16.60%	23.80%	28.00%	21.20%
	AutoAttack- ℓ_2	Clf	99.80%	93.00%	57.00%	5.40%	4.20%
		Pur+Clf	15.40%	14.60%	17.80%	15.60%	14.60%
ImageNet-100	PGD+EOT	Clf	89.40%	86.60%	82.20%	51.20%	26.20%
		Pur+Clf	45.40%	50.20%	57.80%	59.80%	49.40%
	PGD- ℓ_2 +EOT	Clf	94.80%	80.20%	67.00%	31.40%	24.40%
		Pur+Clf	43.60%	45.80%	47.00%	46.60%	45.40%

TABLE VI

STANDARD AND ROBUST ACCURACY AGAINST HIGH INTENSITY ATTACKS WITH $\epsilon = 16/255$ FOR ℓ_∞ -NORM AND $\epsilon = 1$ FOR ℓ_2 -NORM ON CIFAR-10. ALL PURIFICATION METHODS ARE IMPLEMENTED ACCORDING TO THEIR ORIGINAL PARAMETER SETTINGS.

Method	Standard	PGD+EOT	PGD- ℓ_2 +EOT	AutoAttack	AutoAttack- ℓ_2
DiffPure [21]	90.27 \pm 0.81	13.33 \pm 1.33	65.98 \pm 0.47	21.40 \pm 1.04	64.09 \pm 1.59
GNSP [22]	90.40\pm1.40	21.10 \pm 1.32	72.00 \pm 0.71	33.80 \pm 2.40	72.09 \pm 1.80
CMAP (Ours)	88.73 \pm 0.50	64.53\pm1.89	78.33\pm1.17	80.73\pm1.63	80.33\pm1.75

From Fig. 1, two cases (consistency model [15] on CIFAR-10 and diffusion model [16] on ImageNet) demonstrate that the generated samples tend to be closely aligned with clean samples, while remaining significantly distant from adversarial ones. This indicates that the latent space of the generative model is well-aligned with the clean data manifold, enabling the generation of samples that closely resemble clean data and are resistant to adversarial perturbations, underscoring the efficacy of our latent distribution consistency constraint. We also show two more cases in Fig. 7 in Appendix.

C. Comparison on Benchmark Datasets

We compare CMAP with the state-of-the-art adversarial training and purification methods against both ℓ_∞ and ℓ_2 threat models, as shown in Tab. I, II, III and IV.

Results on CIFAR-10. Tab. I reports the defense performance against PGD+EOT and AutoAttack under ℓ_∞ ($\epsilon = 8/255$) and ℓ_2 ($\epsilon = 0.5$) norm constraints on CIFAR-10, over two WideResNet classifiers [83]. Our proposed CMAP demonstrates significant improvements over the latest adversarial training and purification methods against ℓ_∞ attacks, while maintaining comparable performance on ℓ_2 attacks and clean samples. In particular, CMAP surpasses other purification methods by 18.73% against PGD+EOT attack, and achieves improvements ranging from 8.27% to 9.66% on WideResNet-28-10 and WideResNet-70-16, for AutoAttack.

Tab. III shows the results of our CMAP against BPDA+EOT attack. Although our method performs slightly worse than GNSP [22], this could be due to GNSP’s use of an 8-step “Diffusion-Denoising” process, where each step fully applies DiffPure [21]. Notably, our CMAP is also able to incorporate the DiffPure operation by purifying the test sample prior to applying our approach. From Tab. IV, DiffPure further

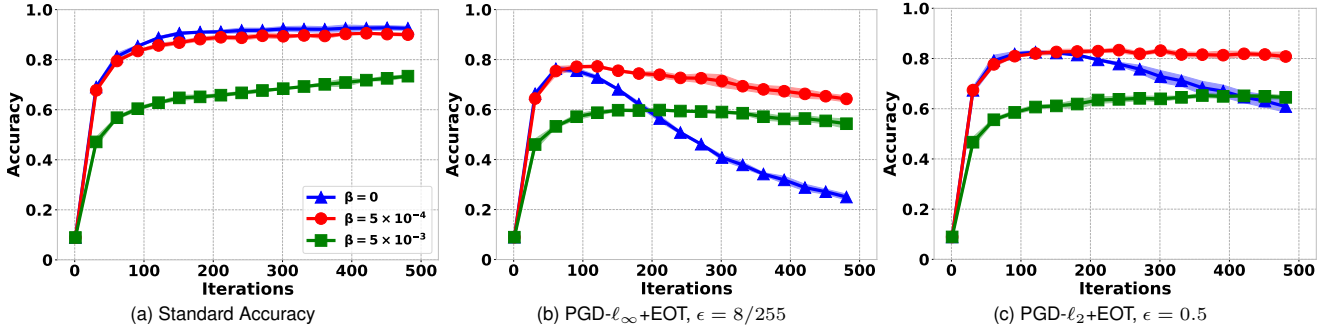


Fig. 3. Standard and robust accuracy curves under different β against PGD+EOT attack with ℓ_∞ -norm ($\epsilon = 8/255$) and ℓ_2 -norm ($\epsilon = 0.5$) on CIFAR-10, where we use WideResNet-28-10 as the classifier. The results indicate that the absence of constraint ($\beta = 0$) leads to a significant drop in robust accuracy, while an excessive constraint ($\beta = 5 \times 10^{-3}$) negatively impacts both standard and robust accuracy. In contrast, $\beta = 5 \times 10^{-4}$ achieves a favorable balance between standard and robust accuracy, thereby simultaneously suppressing adversarial perturbations while maintaining effective image restoration.

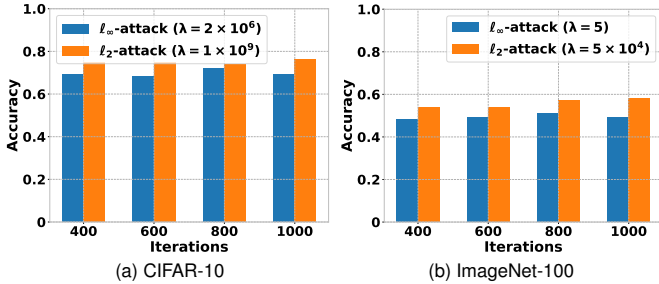


Fig. 4. Robust accuracy across iterations against consistency-disruption attack with ℓ_∞ -norm and ℓ_2 -norm on WideResNet-28-10 for CIFAR-10 and ResNet50 for ImageNet-100. The alignment iterations $T_{\text{def}} = 200$ for CIFAR-10 and $T_{\text{def}} = 300$ for ImageNet-100, with subsequent attack iterations T_{adv} extending to 1000. CMAP maintains high performance throughout the process.

TABLE VII

IMPACT OF THE SIMILARITY FACTOR α ON STANDARD AND ROBUST ACCURACY AGAINST ℓ_∞ ($\epsilon = 8/255$) AND ℓ_2 ($\epsilon = 0.5$) THREAT MODELS, WHERE WE EVALUATE OVER WIDERESNET-28-10 ON CIFAR-10.

Acc \ α	0.5	1	2	5	10
Clean	81.20 \pm 1.31	85.80 \pm 0.53	88.73 \pm 0.50	90.87\pm0.46	90.53 \pm 0.61
PGD+EOT	73.47 \pm 1.55	75.07\pm0.31	74.60 \pm 1.59	68.40 \pm 2.42	63.73 \pm 1.14
PGD- ℓ_2 +EOT	77.53 \pm 2.23	80.93 \pm 1.29	84.00\pm1.71	82.67 \pm 1.62	81.60 \pm 1.25
BPDA+EOT	77.53 \pm 0.61	81.40 \pm 0.35	83.53\pm1.80	80.60 \pm 1.40	78.53 \pm 1.55

enhances the robustness of our CMAP against AutoAttack- ℓ_2 and BPDA+EOT. In addition, while adversarial training outperforms adversarial purification in some cases, it exhibits a significant decline in robustness against unseen attacks [21].

Results on ImageNet-100. As shown in Tab. II and III, our CMAP consistently outperforms state-of-the-art purification methods in both robust accuracy and standard accuracy on ImageNet-100 under ℓ_∞ ($\epsilon = 4/255$) and ℓ_2 ($\epsilon = 0.5$) attacks. In particular, CMAP achieves absolute improvements in robust accuracy ranging from 6.47% to 8.79% for PGD+EOT attacks, from 0.62% to 3.74% for PGD- ℓ_2 +EOT and 0.79% for BPDA+EOT across different classifiers. Moreover, the standard accuracy also increases by 1.15% to 2.01%.

The results clearly show the effectiveness of CMAP across various architectures and datasets in defending different attacks. Notably, CMAP is agnostic to classifier architectures or attack types, employing a unified defense operation, *e.g.*, optimization iterations T . This contrasts with prior purification methods [20]–[22], which require different hyperparameters, *e.g.*, the diffusion timestep t_{diff} , for different attacks.

TABLE VIII

IMPACT OF THE GAUSSIAN FACTOR β ON STANDARD AND ROBUST ACCURACY AGAINST ℓ_∞ ($\epsilon = 8/255$) AND ℓ_2 ($\epsilon = 0.5$) THREAT MODELS, WHERE WE EVALUATE ON WIDERESNET-28-10 FOR CIFAR-10.

Acc \ β	1×10^{-4}	2×10^{-4}	5×10^{-4}	1×10^{-3}	2×10^{-3}
Clean	91.53\pm0.31	90.87 \pm 0.64	88.73 \pm 0.50	85.73 \pm 0.81	80.67 \pm 1.29
PGD+EOT	65.07 \pm 1.90	69.27 \pm 2.60	74.60\pm1.59	74.27 \pm 1.60	71.20 \pm 0.35
PGD- ℓ_2 +EOT	82.00 \pm 0.69	83.00 \pm 1.93	84.00\pm1.71	80.67 \pm 1.22	74.40 \pm 2.84
BPDA+EOT	78.73 \pm 0.81	80.67 \pm 1.21	83.53\pm1.80	80.20 \pm 2.36	75.67 \pm 0.42

TABLE IX

IMPACT OF THE LATENT VECTOR NUMBER K ON STANDARD AND ROBUST ACCURACY AGAINST ℓ_∞ ($\epsilon = 8/255$) AND ℓ_2 ($\epsilon = 0.5$) THREAT MODELS, WHERE WE EVALUATE ON WIDERESNET-28-10 FOR CIFAR-10.

Acc \ K	2	5	10	20
Clean	80.13 \pm 1.17	87.27 \pm 1.10	88.73 \pm 0.50	89.27\pm0.42
PGD+EOT	69.67 \pm 2.19	73.67 \pm 1.40	74.60\pm1.59	73.40 \pm 1.64
PGD- ℓ_2 +EOT	76.80 \pm 3.27	81.20 \pm 1.74	84.00\pm1.71	83.53 \pm 1.14
BPDA+EOT	76.13 \pm 2.57	81.53 \pm 1.75	83.53\pm1.80	82.47 \pm 1.30

D. Purification on High Attack Intensity

To further demonstrate the superiority of our CMAP, we conduct experiments under conditions of extremely high attack intensity on CIFAR-10, *i.e.*, using $\epsilon = 16/255$ for ℓ_∞ -norm attacks and $\epsilon = 1$ for ℓ_2 -norm attacks. As shown in Tab. VI, the diffusion-based purification baselines suffer from significant performance degradation. In contrast, our CMAP exhibits remarkable robustness, achieving improvements ranging from 43.43% to 46.93% for ℓ_∞ -norm threats and 6.33% to 8.24% for ℓ_2 -norm threats. The results indicate that CMAP effectively maintains features of the clean data while removing adversarial noise, even under intense attack scenarios. This suggests that the latent space optimization by our method is more robust to high-intensity adversarial attacks, maintaining a stable purification process even under severe perturbations.

E. Defense against Consistency-Disruption Attack

To further evaluate the robustness of our CMAP, we apply the consistency-disruption attack in Sec. IV-D to our CMAP. This attack targets all components of CMAP and generates K adversarial samples for each clean sample, aligned with the procedure of CMAP. The attack is successful if any of these samples lead to a misclassification after performing our defense, and λ is set to yield the lowest purification accuracy (see Tab.

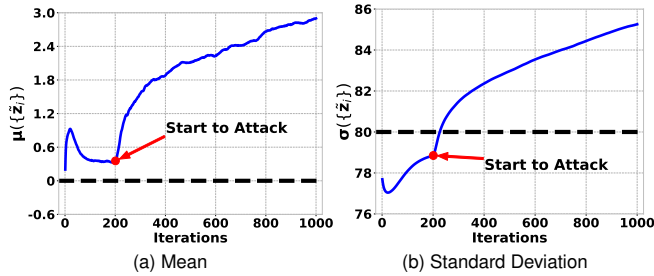


Fig. 5. Mean and standard deviation of optimized latent vectors by consistency-disruption attack ($\epsilon = 8/255$) across optimization iterations on CIFAR-10, where $\mu = 0$ and $\sigma = 80$ are the mean and variance of the latent distribution.

TABLE X

ROBUST ACCURACY AGAINST THE CONSISTENCY-DISRUPTION ATTACK UNDER DIFFERENT HYPER-PARAMETER λ . λ IS CHOSEN TO ACHIEVE THE LOWEST ACCURACY (I.E., THE HIGHEST ATTACK INTENSITY).

Dataset	ℓ_∞	λ	5×10^5	1×10^6	2×10^6	5×10^6	1×10^7
			CIFAR-10	(8/255)	Acc	71.00	69.00
	ℓ_2	λ	2×10^8	5×10^8	1×10^9	2×10^9	5×10^9
			CIFAR-10	(0.5)	Acc	73.00	73.00
	ℓ_∞	λ	1	2	5	10	20
			ImageNet-100	(4/255)	Acc	51.00	47.00
	ℓ_2	λ	1×10^4	2×10^4	5×10^4	1×10^5	2×10^5
			ImageNet-100	(0.5)	Acc	54.00	54.00

X). For this evaluation, we report the robust accuracy across optimization iterations. As shown in Fig. 4, our CMAP still maintains strong robust accuracy throughout the attack process across both datasets and against ℓ_2 or ℓ_∞ attacks.

To explore the underlying reason for successful purification by our CMAP, we report the mean and variance of latent vectors over iterations, as depicted in Fig. 5. As the attack starts, the distribution of the K latent vectors rapidly deviates from the latent distribution of the pre-trained consistency model. However, this deviation is effectively corrected by our latent distribution consistency constraint mechanism, guiding the generated samples back toward the clean data manifold.

F. Ablation Studies

The preceding results show the satisfactory robustness of our CMAP against both white-box attacks and consistency-disruption attack. This stems from three key components: 1) the perceptual consistency restoration, capturing fine textures and details of the test sample; 2) the latent distribution consistency constraint, effectively avoiding fitting adversarial perturbations; 3) the latent vector consistency prediction, aggregating multiple generated samples for more reliable classification outcomes. Next, we validate the effectiveness of each related component.

Impact of the perceptual consistency restoration. Both mean absolute error (MAE) and structure similarity index measure (SSIM) are used to restore test samples from latent vectors, with a factor α to balance these terms. We demonstrate the effect of α over WideResNet-28-10 on CIFAR-10 in Tab. VII. Notably, as α increases, both standard and adversarial accuracy gradually improve, indicating that introducing the SSIM term during restoration accelerates alignment optimization. However, when α becomes too large, e.g., $\alpha > 2$, both

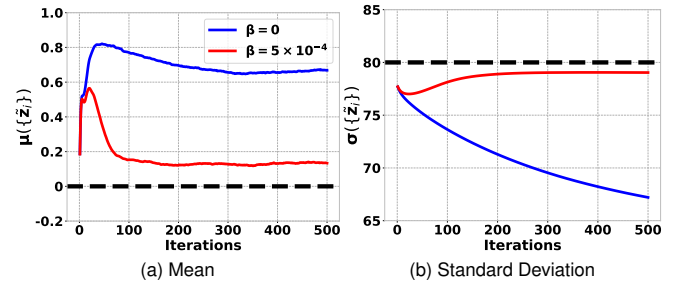


Fig. 6. Mean and standard deviation of optimized latent vectors by our CMAP in Alg. 1 across optimization iterations under different β on CIFAR-10 against PGD+EOT attack with $\epsilon = 8/255$.

TABLE XI

STANDARD AND ROBUST ACCURACY AGAINST PGD+EOT AND AUTOATTACK WITH ℓ_∞ -NORM ON CIFAR-10 ($\epsilon = 8/255$) AND IMAGENET-100 ($\epsilon = 4/255$). THE LATENT VECTOR CONSISTENCY PREDICTION ENHANCES BOTH STANDARD AND ROBUST ACCURACY.

Dataset	Classifier	Method	Standard	PGD+EOT	AutoAttack
CIFAR-10	WRN-28-10	CMAP w/o Vote	83.07 \pm 0.50	69.87 \pm 2.14	72.07 \pm 2.00
		CMAP w/ Vote	88.73\pm0.50	74.60\pm1.59	78.67\pm1.90
	WRN-70-16	CMAP w/o Vote	82.44 \pm 0.92	70.66 \pm 1.14	75.23 \pm 0.42
		CMAP w/ Vote	88.27\pm0.50	74.80\pm1.56	81.33\pm0.31
ImageNet-100	ResNet50	CMAP w/o Vote	58.72 \pm 1.71	38.20 \pm 1.35	—
		CMAP w/ Vote	61.53\pm1.45	39.27\pm1.79	—

robust and clean accuracy start to decline. This may result from an excessive focus on structural similarity at the expense of pixel-wise alignment, reducing the model’s ability to generalize effectively to both adversarial and clean samples.

Impact of the latent distribution consistency constraint. The coefficient β controls the strength of the latent distribution consistency constraint. To investigate its impact, we plot the standard and robust accuracy across iterations with different β in Fig. 3. Without the distribution constraint, i.e., $\beta = 0$, the restoration exhibits a significant decline in robust accuracy after reaching a peak, especially for PGD- ℓ_∞ +EOT. In contrast, it remains stable throughout the optimization with $\beta = 5 \times 10^{-4}$. Additionally, an excessively strong distribution constraint can impair the restoration of the test sample, as evidenced by reduced peak performance at $\beta = 5 \times 10^{-3}$. More quantitative results in Tab. VIII further support these observations. Thus, we set $\beta = 5 \times 10^{-4}$ that simultaneously suppresses adversarial perturbations while maintaining effective image restoration.

Furthermore, to delve into the mechanism behind the latent distribution consistency constraint, we examine its effect on latent vectors during optimization. To this end, we depict the mean and standard deviation of the latent vectors throughout the optimization process. As illustrated in Fig. 6, without the distribution constraint, i.e., $\beta = 0$, the mean and standard deviation of the optimized latent vectors deviate significantly from the latent distribution, where the dotted lines represent the referenced statistics w.r.t. the latent distribution.

Impact of the number of latent vectors K . The effectiveness of the latent distribution consistency constraint is also influenced by the number of latent vectors initialized for optimization, denoted as K . Intuitively, increasing K reduces the bias in the estimation of mean and variance, thereby reinforcing the distribution constraint and leading to improved

optimization outcomes. However, a larger K comes with a linearly increasing computational cost. As shown in Tab. IX, both standard and robust accuracy generally improve with larger K . Nevertheless, when $K = 20$, robust accuracy exhibits a slight decline. This issue can be alleviated by further adjusting β . However, to adhere to the principle of controlling for a single variable in ablation studies, we maintain consistent parameter settings in the reported results. Taking both performance and computational efficiency into account, we select $K = 10$ for CIFAR-10 and $K = 5$ for ImageNet-100.

Impact of the latent vector consistency prediction. We ablate the impact of the latent vector consistency prediction by randomly selecting one of the K samples for prediction. As shown in Tab. XI, this mechanism improves standard and robust accuracy by 4.14% to 6.60% on CIFAR-10, and by 1.07% to 2.81% on ImageNet-100, respectively. Notably, the performance without voting remains at an acceptable level (surpassing the DiffPure [21]), verifying the effectiveness of the entire purification process. Nevertheless, since our method already optimizes K latent vectors, leveraging this information through voting is a natural and effective choice.

VI. CONCLUSION AND FUTURE WORK

In this paper, we reveal that samples from a well-trained generative model are close to clean ones but far from adversarial ones. Leveraging this, we propose a Consistency Model-based Adversarial Purification (CMAP) method. By integrating a perceptual consistency restoration mechanism and a latent distribution consistency constraint strategy, our CMAP aligns the generated samples with the clean data manifold while preserving essential high-level perceptual features. Additionally, the latent vector consistency prediction scheme improves the stability and reliability of the final predictions. We also apply a consistency-disruption attack that takes into account the overall defense mechanism, aiming to exploit potential vulnerabilities. Extensive experiments on CIFAR-10 and ImageNet-100 across various classifier architectures such as ResNet and WideResNet demonstrate that our method achieves superior performance in robust and standard accuracy under diverse attack scenarios.

Future work. While our CMAP demonstrates superior robustness, its computational efficiency can be improved. Currently, our approach requires optimizing K latent vectors for each test sample, with $K = 10$ for CIFAR-10 and $K = 5$ for ImageNet-100, balancing robustness and computational cost. Future work could explore more efficient optimization strategies, potentially reducing iterations or designing lightweight consistency models to lower computational burden. Additionally, adaptive mechanisms that dynamically adjust the number of latent vectors based on input or attack intensity could further improve both performance and efficiency, making CMAP more scalable for real-time applications.

REFERENCES

- [1] K. He, X. Zhang, S. Ren, and J. Sun, "Deep residual learning for image recognition," in *CVPR*, pp. 770–778, 2016.
- [2] Y. Pei, Y. Huang, Q. Zou, X. Zhang, and S. Wang, "Effects of image degradation and degradation removal to cnn-based image classification," *IEEE Transactions on Pattern Analysis and Machine Intelligence (TPAMI)*, vol. 43, no. 4, pp. 1239–1253, 2019.
- [3] D. Bahdanau, K. Cho, and Y. Bengio, "Neural machine translation by jointly learning to align and translate," in *ICLR*, 2015.
- [4] E. De Santis, A. Martino, and A. Rizzi, "Human versus machine intelligence: Assessing natural language generation models through complex systems theory," *IEEE Transactions on Pattern Analysis and Machine Intelligence (TPAMI)*, vol. 46, no. 7, pp. 4812–4829, 2024.
- [5] A. Baevski, W. Hsu, A. Conneau, and M. Auli, "Unsupervised speech recognition," in *NeurIPS*, 2021.
- [6] T. Afouras, J. S. Chung, A. Senior, O. Vinyals, and A. Zisserman, "Deep audio-visual speech recognition," *IEEE Transactions on Pattern Analysis and Machine Intelligence (TPAMI)*, vol. 44, no. 12, pp. 8717–8727, 2018.
- [7] B. Lin, Y. Long, Y. Zhu, F. Zhu, X. Liang, Q. Ye, and L. Lin, "Towards deviation-robust agent navigation via perturbation-aware contrastive learning," *IEEE Transactions on Pattern Analysis and Machine Intelligence (TPAMI)*, vol. 45, no. 10, pp. 12535–12549, 2023.
- [8] I. J. Goodfellow, J. Shlens, and C. Szegedy, "Explaining and harnessing adversarial examples," in *ICLR*, 2015.
- [9] B. Chen, Y. Feng, T. Dai, J. Bai, Y. Jiang, S.-T. Xia, and X. Wang, "Adversarial examples generation for deep product quantization networks on image retrieval," *IEEE Transactions on Pattern Analysis and Machine Intelligence (TPAMI)*, vol. 45, no. 2, pp. 1388–1404, 2022.
- [10] A. Arnab, O. Miksik, and P. H. S. Torr, "On the robustness of semantic segmentation models to adversarial attacks," *IEEE Transactions on Pattern Analysis and Machine Intelligence (TPAMI)*, vol. 42, no. 12, pp. 3040–3053, 2020.
- [11] J. Wu, Y. Zhou, H. Yang, Z. Huang, and C. Lv, "Human-guided reinforcement learning with sim-to-real transfer for autonomous navigation," *IEEE Transactions on Pattern Analysis and Machine Intelligence (TPAMI)*, vol. 45, no. 12, pp. 14745–14759, 2023.
- [12] X. Wang, W. Wang, J. Shao, and Y. Yang, "Learning to follow and generate instructions for language-capable navigation," *IEEE Transactions on Pattern Analysis and Machine Intelligence (TPAMI)*, vol. 46, no. 5, pp. 3334–3350, 2024.
- [13] U. Ozbulak, A. Van Messem, and W. De Neve, "Impact of adversarial examples on deep learning models for biomedical image segmentation," in *MICCAI*, 2019.
- [14] G. Zhao, Q. Feng, C. Chen, Z. Zhou, and Y. Yu, "Diagnose like a radiologist: Hybrid neuro-probabilistic reasoning for attribute-based medical image diagnosis," *IEEE Transactions on Pattern Analysis and Machine Intelligence (TPAMI)*, vol. 44, no. 11, pp. 7400–7416, 2021.
- [15] Y. Song, P. Dhariwal, M. Chen, and I. Sutskever, "Consistency models," in *ICML*, pp. 32211–32252, PMLR, 2023.
- [16] P. Dhariwal and A. Nichol, "Diffusion models beat gans on image synthesis," in *NeurIPS*, vol. 34, pp. 8780–8794, 2021.
- [17] A. Gretton, K. M. Borgwardt, M. J. Rasch, B. Schölkopf, and A. Smola, "A kernel two-sample test," *Journal of Machine Learning Research (JMLR)*, vol. 13, no. 1, pp. 723–773, 2012.
- [18] A. Madry, A. Makelov, L. Schmidt, D. Tsipras, and A. Vladu, "Towards deep learning models resistant to adversarial attacks," *arXiv preprint arXiv:1706.06083*, 2017.
- [19] S. Goyal, S.-A. Rebuffi, O. Wiles, F. Stimberg, D. A. Calian, and T. A. Mann, "Improving robustness using generated data," in *NeurIPS*, vol. 34, pp. 4218–4233, 2021.
- [20] J. Yoon, S. J. Hwang, and J. Lee, "Adversarial purification with score-based generative models," in *ICML*, pp. 12062–12072, PMLR, 2021.
- [21] W. Nie, B. Guo, Y. Huang, C. Xiao, A. Vahdat, and A. Anandkumar, "Diffusion models for adversarial purification," in *ICML*, pp. 16805–16827, PMLR, 2022.
- [22] M. Lee and D. Kim, "Robust evaluation of diffusion-based adversarial purification," in *ICCV*, pp. 134–144, 2023.
- [23] T. Pang, M. Lin, X. Yang, J. Zhu, and S. Yan, "Robustness and accuracy could be reconcilable by (proper) definition," in *ICML*, pp. 17258–17277, PMLR, 2022.
- [24] H. Zheng, Z. Zhang, J. Gu, H. Lee, and A. Prakash, "Efficient adversarial training with transferable adversarial examples," in *CVPR*, pp. 1181–1190, 2020.
- [25] P. de Jorge Aranda, A. Bibi, R. Volpi, A. Sanyal, P. Torr, G. Rogez, and P. Dokania, "Make some noise: Reliable and efficient single-step adversarial training," in *NeurIPS*, vol. 35, pp. 12881–12893, 2022.
- [26] E. Wong, L. Rice, and J. Z. Kolter, "Fast is better than free: Revisiting adversarial training," in *ICLR*, 2020.
- [27] C. Shi, C. Holtz, and G. Mishne, "Online adversarial purification based on self-supervised learning," in *ICLR*, 2021.
- [28] M. Hill, J. C. Mitchell, and S.-C. Zhu, "Stochastic security: Adversarial defense using long-run dynamics of energy-based models," in *ICLR*, 2021.

- [29] I. Goodfellow, J. Pouget-Abadie, M. Mirza, B. Xu, D. Warde-Farley, S. Ozair, A. Courville, and Y. Bengio, "Generative adversarial nets," in *NeurIPS*, vol. 27, 2014.
- [30] Y. LeCun, S. Chopra, R. Hadsell, M. Ranzato, F. Huang, *et al.*, "A tutorial on energy-based learning," *Predicting structured data*, vol. 1, no. 0, 2006.
- [31] Y. Song and S. Ermon, "Generative modeling by estimating gradients of the data distribution," in *NeurIPS*, vol. 32, 2019.
- [32] R. Rombach, A. Blattmann, D. Lorenz, P. Esser, and B. Ommer, "High-resolution image synthesis with latent diffusion models," in *CVPR*, pp. 10684–10695, 2022.
- [33] A. Ramesh, P. Dhariwal, A. Nichol, C. Chu, and M. Chen, "Hierarchical text-conditional image generation with clip latents," *arXiv preprint arXiv:2204.06125*, 2022.
- [34] J. Ho, A. Jain, and P. Abbeel, "Denosing diffusion probabilistic models," in *NeurIPS*, vol. 33, pp. 6840–6851, 2020.
- [35] C. J. Willmott and K. Matsuura, "Advantages of the mean absolute error (mae) over the root mean square error (rmse) in assessing average model performance," *Climate research*, vol. 30, no. 1, pp. 79–82, 2005.
- [36] D. Brunet, E. R. Vrscay, and Z. Wang, "On the mathematical properties of the structural similarity index," *IEEE Transactions on Image Processing (TIP)*, vol. 21, no. 4, pp. 1488–1499, 2011.
- [37] J. Wang, Z. Lyu, D. Lin, B. Dai, and H. Fu, "Guided diffusion model for adversarial purification," *arXiv preprint arXiv:2205.14969*, 2022.
- [38] A. Prakash, N. Moran, S. Garber, A. DiLillo, and J. Storer, "Deflecting adversarial attacks with pixel deflection," in *CVPR*, pp. 8571–8580, 2018.
- [39] X. Yuan, P. He, Q. Zhu, and X. Li, "Adversarial examples: Attacks and defenses for deep learning," *IEEE Transactions on Neural Networks and Learning Systems (TNNLS)*, vol. 30, no. 9, pp. 2805–2824, 2019.
- [40] H. Zhao, O. Gallo, I. Frosio, and J. Kautz, "Loss functions for image restoration with neural networks," *IEEE Transactions on Computational Imaging (TCI)*, vol. 3, no. 1, pp. 47–57, 2016.
- [41] Z. Wang and A. C. Bovik, "Mean squared error: Love it or leave it? a new look at signal fidelity measures," *IEEE Signal Processing Magazine (IEEE SPM)*, vol. 26, no. 1, pp. 98–117, 2009.
- [42] C. Xiao, Z. Chen, K. Jin, J. Wang, W. Nie, M. Liu, A. Anandkumar, B. Li, and D. Song, "Densepure: Understanding diffusion models for adversarial robustness," in *ICLR*, 2023.
- [43] F. Croce and M. Hein, "Reliable evaluation of adversarial robustness with an ensemble of diverse parameter-free attacks," in *ICML*, pp. 2206–2216, PMLR, 2020.
- [44] A. Athalye, L. Engstrom, A. Ilyas, and K. Kwok, "Synthesizing robust adversarial examples," in *ICML*, pp. 284–293, PMLR, 2018.
- [45] Y. Song and S. Ermon, "Improved techniques for training score-based generative models," in *NeurIPS*, vol. 33, pp. 12438–12448, 2020.
- [46] Y. Song, J. Sohl-Dickstein, D. P. Kingma, A. Kumar, S. Ermon, and B. Poole, "Score-based generative modeling through stochastic differential equations," in *ICLR*, 2021.
- [47] J. Sohl-Dickstein, E. Weiss, N. Maheswaranathan, and S. Ganguli, "Deep unsupervised learning using nonequilibrium thermodynamics," in *ICML*, pp. 2256–2265, PMLR, 2015.
- [48] S. Jiaming, M. Chenlin, and E. Stefano, "Denosing diffusion implicit models," in *ICLR*, 2021.
- [49] C. Lu, Y. Zhou, F. Bao, J. Chen, C. Li, and J. Zhu, "Dpm-solver: A fast ode solver for diffusion probabilistic model sampling in around 10 steps," in *NeurIPS*, vol. 35, pp. 5775–5787, 2022.
- [50] S. Tim and H. Jonathan, "Progressive distillation for fast sampling of diffusion models," in *ICLR*, 2022.
- [51] I. J. Goodfellow, J. Shlens, and C. Szegedy, "Explaining and harnessing adversarial examples," in *ICLR*, 2015.
- [52] A. Athalye, N. Carlini, and D. Wagner, "Obfuscated gradients give a false sense of security: Circumventing defenses to adversarial examples," in *ICML*, pp. 274–283, PMLR, 2018.
- [53] C. Szegedy, W. Zaremba, I. Sutskever, J. Bruna, D. Erhan, I. J. Goodfellow, and R. Fergus, "Intriguing properties of neural networks," in *ICLR*, 2014.
- [54] N. Papernot, P. McDaniel, S. Jha, M. Fredrikson, Z. B. Celik, and A. Swami, "The limitations of deep learning in adversarial settings," in *IEEE European symposium on Security and Privacy (EuroS&P)*, pp. 372–387, IEEE, 2016.
- [55] R. Huang, B. Xu, D. Schuurmans, and C. Szepesvári, "Learning with a strong adversary," *arXiv preprint arXiv:1511.03034*, 2015.
- [56] U. Shaham, Y. Yamada, and S. Negahban, "Understanding adversarial training: Increasing local stability of supervised models through robust optimization," *Neurocomputing*, vol. 307, pp. 195–204, 2018.
- [57] H. Zhang, Y. Yu, J. Jiao, E. Xing, L. El Ghaoui, and M. Jordan, "Theoretically principled trade-off between robustness and accuracy," in *ICML*, pp. 7472–7482, PMLR, 2019.
- [58] P. Samangouei, M. Kabkab, and R. Chellappa, "Defense-GAN: Protecting classifiers against adversarial attacks using generative models," in *ICLR*, 2018.
- [59] Y. Song, T. Kim, S. Nowozin, S. Ermon, and N. Kushman, "Pixeldefend: Leveraging generative models to understand and defend against adversarial examples," in *ICLR*, 2018.
- [60] V. Srinivasan, C. Rohrer, A. Marban, K.-R. Müller, W. Samek, and S. Nakajima, "Robustifying models against adversarial attacks by langevin dynamics," *Neural Networks*, vol. 137, pp. 1–17, 2021.
- [61] G. O. Roberts and J. S. Rosenthal, "Optimal scaling of discrete approximations to langevin diffusions," *Journal of the Royal Statistical Society: Series B (Statistical Methodology)*, vol. 60, no. 1, pp. 255–268, 1998.
- [62] Y. Du and I. Mordatch, "Implicit generation and modeling with energy based models," in *NeurIPS*, vol. 32, 2019.
- [63] W. Grathwohl, K.-C. Wang, J.-H. Jacobsen, D. Duvenaud, M. Norouzi, and K. Swersky, "Your classifier is secretly an energy based model and you should treat it like one," in *ICLR*, 2020.
- [64] M. Hill, J. C. Mitchell, and S.-C. Zhu, "Stochastic security: Adversarial defense using long-run dynamics of energy-based models," in *ICLR*, 2021.
- [65] P. Samangouei, M. Kabkab, and R. Chellappa, "Defense-gan: Protecting classifiers against adversarial attacks using generative models," in *ICLR*, 2018.
- [66] B. D. Anderson, "Reverse-time diffusion equation models," *Stochastic Processes and their Applications*, vol. 12, no. 3, pp. 313–326, 1982.
- [67] W. Xia, Y. Zhang, Y. Yang, J.-H. Xue, B. Zhou, and M.-H. Yang, "GAN inversion: A survey," *IEEE Transactions on Pattern Analysis and Machine Intelligence (TPAMI)*, vol. 45, no. 3, pp. 3121–3138, 2022.
- [68] D. Roich, R. Mokady, A. H. Bermano, and D. Cohen-Or, "Pivotal tuning for latent-based editing of real images," *ACM Transactions on Graphics (TOG)*, vol. 42, no. 1, pp. 1–13, 2022.
- [69] O. Avrahami, O. Fried, and D. Lischinski, "Blended latent diffusion," *ACM transactions on graphics (TOG)*, vol. 42, no. 4, pp. 1–11, 2023.
- [70] P. Schramowski, M. Brack, B. Deiseroth, and K. Kersting, "Safe latent diffusion: Mitigating inappropriate degeneration in diffusion models," in *CVPR*, pp. 22522–22531, 2023.
- [71] M. Xu, A. S. Powers, R. O. Dror, S. Ermon, and J. Leskovec, "Geometric latent diffusion models for 3d molecule generation," in *ICML*, pp. 38592–38610, PMLR, 2023.
- [72] A.-K. Dombrowski, J. E. Gerken, K.-R. Müller, and P. Kessel, "Diffeomorphic counterfactuals with generative models," *IEEE Transactions on Pattern Analysis and Machine Intelligence (TPAMI)*, 2023.
- [73] C. Villani *et al.*, *Optimal transport: old and new*, vol. 338. Springer, 2009.
- [74] K. M. Borgwardt, A. Gretton, M. J. Rasch, H.-P. Kriegel, B. Schölkopf, and A. J. Smola, "Integrating structured biological data by kernel maximum mean discrepancy," *Bioinformatics*, vol. 22, no. 14, pp. e49–e57, 2006.
- [75] H. Qin, Y. Ding, X. Zhang, J. Wang, X. Liu, and J. Lu, "Diverse sample generation: Pushing the limit of generative data-free quantization," *IEEE Transactions on Pattern Analysis and Machine Intelligence (TPAMI)*, vol. 45, no. 10, pp. 11689–11706, 2023.
- [76] H. Yin, P. Molchanov, J. M. Alvarez, Z. Li, A. Mallya, D. Hoiem, N. K. Jha, and J. Kautz, "Dreaming to distill: Data-free knowledge transfer via deepinversion," in *CVPR*, pp. 8715–8724, 2020.
- [77] S. Goyal, C. Qin, J. Uesato, T. Mann, and P. Kohli, "Uncovering the limits of adversarial training against norm-bounded adversarial examples," *arXiv preprint arXiv:2010.03593*, 2020.
- [78] S.-A. Rebuffi, S. Goyal, D. A. Calian, F. Stimberg, O. Wiles, and T. Mann, "Fixing data augmentation to improve adversarial robustness," *arXiv preprint arXiv:2103.01946*, 2021.
- [79] M. Augustin, A. Meinke, and M. Hein, "Adversarial robustness on in- and out-distribution improves explainability," in *ECCV*, pp. 228–245, Springer, 2020.
- [80] V. Sehwag, S. Mahlouiifar, T. Handina, S. Dai, C. Xiang, M. Chiang, and P. Mittal, "Robust learning meets generative models: Can proxy distributions improve adversarial robustness?," in *ICLR*, 2022.
- [81] A. Krizhevsky, G. Hinton, *et al.*, "Learning multiple layers of features from tiny images," *Technical Report*, 2009.
- [82] O. Russakovsky, J. Deng, H. Su, J. Krause, S. Satheesh, S. Ma, Z. Huang, A. Karpathy, A. Khosla, M. Bernstein, *et al.*, "Imagenet large scale visual recognition challenge," *International Journal of Computer Vision (IJCV)*, vol. 115, pp. 211–252, 2015.

- [83] S. Zagoruyko and N. Komodakis, “Wide residual networks,” in *BMVC*, 2016.
- [84] Z. Liu, S. Li, D. Wu, Z. Chen, L. Wu, J. Guo, and S. Z. Li, “Automix: Unveiling the power of mixup for stronger classifiers,” in *ECCV*, pp. 441–458, 2022.
- [85] T. Karras, M. Aittala, T. Aila, and S. Laine, “Elucidating the design space of diffusion-based generative models,” in *NeurIPS*, vol. 35, pp. 26565–26577, 2022.
- [86] F. Croce, M. Andriushchenko, V. Schwag, E. Debenedetti, N. Flammarion, M. Chiang, P. Mittal, and M. Hein, “Robustbench: a standardized adversarial robustness benchmark,” in *NeurIPS*, 2021.
- [87] R. Gao, F. Liu, J. Zhang, B. Han, T. Liu, G. Niu, and M. Sugiyama, “Maximum mean discrepancy test is aware of adversarial attacks,” in *ICML*, pp. 3564–3575, PMLR, 2021.
- [88] S. Zhang, F. Liu, J. Yang, Y. Yang, C. Li, B. Han, and M. Tan, “Detecting adversarial data by probing multiple perturbations using expected perturbation score,” in *ICML*, 2023.
- [89] A. Q. Nichol and P. Dhariwal, “Improved denoising diffusion probabilistic models,” in *ICML*, pp. 8162–8171, PMLR, 2021.
- [90] N. Ikeda, S. Watanabe, M. Fukushima, and H. Kunita, *Itô’s stochastic calculus and probability theory*. Springer Science & Business Media, 2012.
- [91] T. Karras, “Progressive growing of gans for improved quality, stability, and variation,” in *ICLR*, 2018.
- [92] A. Brock, J. Donahue, and K. Simonyan, “Large scale GAN training for high fidelity natural image synthesis,” in *ICLR*, 2019.



Shuhai Zhang is currently a Ph.D. candidate at South China University of Technology in Guangzhou, China. His research interests are broadly in machine learning and mainly focus on trustworthy machine learning. He has published papers in ICML, NeurIPS, ICLR, CVPR, ICCV, TCSVT, Neural Networks.



Jiahao Yang is currently a Master student at South China University of Technology in Guangzhou, China. He received his Bachelor Degree in the School of Mathematics in 2022 from South China University of Technology in Guangzhou, China. His research interests are broadly in machine learning and mainly focus on trustworthy machine learning.



Hui Luo is currently pursuing a Ph.D. in signal and information processing at the University of Chinese Academy of Sciences in Beijing, China. During his Ph.D. program, he also conducts research at the Institute of Optics and Electronics, Chinese Academy of Sciences, located in Chengdu, China. His research interests include model compression and acceleration, and the development of robust and reliable models.

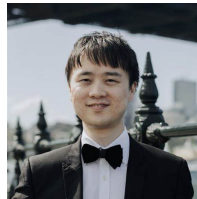


Jie Chen (Member, IEEE) received the MSc and PhD degrees from the Harbin Institute of Technology, China, in 2002 and 2007, respectively. He joined the Shenzhen Graduate School, Peking University, as a faculty member in 2019 and is currently an associate professor with the School of Electronic and Computer Engineering, Peking University. Since 2018, he has been working with the Peng Cheng Laboratory, China. From 2007 to 2018, he worked as a senior researcher with the Center for Machine Vision and Signal Analysis, University of Oulu, Finland. In 2012 and

2015, he visited the Computer Vision Laboratory, University of Maryland, and School of Electrical and Computer Engineering, Duke University, respectively. He was a co-chair of International Workshops at ACCV, CVPR, ICCV, and ECCV. He was a guest editor of special issues for IEEE Transactions on Pattern Analysis and Machine Intelligence, IJCV, and Neurocomputing. His research interests include deep learning, computer vision, and medical image analysis. He is an associate editor of the Visual Computer.

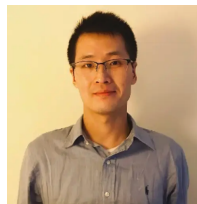


Li Wang received the B.S. degree in information and computing science from China University of Mining and Technology, Jiangsu, China, in 2006, the M.S. degree from Xi’an Jiaotong University, Xi’an, Shaanxi, China, in 2009, and the Ph.D. degree from the Department of Mathematics, University of California at San Diego, San Diego, CA, USA, in 2014. She was a Research Assistant Professor with the Department of Mathematics, Statistics, and Computer Science, University of Illinois at Chicago, Chicago, IL, USA, from 2015 to 2017, and a Post-Doctoral Fellow with the University of Victoria, Victoria, BC, Canada, in 2015, and Brown University, Providence, RI, USA, in 2014. She is currently an Assistant Professor with the Department of Mathematics, The University of Texas at Arlington, Texas, USA, and also with the Department of Computer Science and Engineering. Her research interests include large-scale optimization, polynomial optimization, and machine learning.



Feng Liu (Member, IEEE) received the B.Sc. degree in mathematics and the M.Sc. degree in probability and statistics from the School of Mathematics and Statistics, Lanzhou University, Lanzhou, China, in 2013 and 2013, respectively, and the Ph.D. degree in computer science from the University of Technology Sydney, Sydney, NSW, Australia, in 2020. He is currently a Lecturer with the School of Mathematics and Statistics, Faculty of Science, The University of Melbourne, Melbourne, VIC, Australia. He is also a Visiting Fellow of Australian Artificial Intelligence

Institute, Faculty of Engineering and Information Technology, University of Technology Sydney. His research interests include hypothesis testing and trustworthy machine learning. He has served as a Senior Program Committee Member for ECAI and a Program Committee Member for NeurIPS, ICML, AISTATS, ICLR, KDD, AAAI, IJCAI, and FUZZ-IEEE. He also served as a reviewer for JMLR, MLJ, TPAMI, TNNLS and TFS. He received the Outstanding Reviewer Awards of ICLR in 2021 and NeurIPS in 2021, the UTS-FEIT HDR Research Excellence Award in 2019, and the Best Student Paper Award of FUZZ-IEEE in 2019.



Bo Han is currently an Assistant Professor in Machine Learning at Hong Kong Baptist University, and a BAIHO Visiting Scientist of Imperfect Information Learning Team at RIKEN Center for Advanced Intelligence Project (RIKEN AIP), where his research focuses on machine learning, deep learning, foundation models, and their applications. He was a Visiting Research Scholar at MBZUAI MLD (2024), a Visiting Faculty Researcher at Microsoft Research (2022) and Alibaba DAMO Academy (2021), and a Postdoc Fellow at RIKEN AIP (2019-2020). He

received his Ph.D. degree in Computer Science from University of Technology Sydney (2015-2019). He has served as Senior Area Chair of NeurIPS, and Area Chairs of NeurIPS, ICML and ICLR. He has also served as Associate Editors of IEEE TPAMI, MLJ and JAIR, and Editorial Board Members of JMLR and MLJ. He received Outstanding Paper Award at NeurIPS, Most Influential Paper at NeurIPS, Notable Area Chair at NeurIPS, Outstanding Area Chair at ICLR, and Outstanding Associate Editor at IEEE TNNLS.



Mingkui Tan is currently a Professor with the School of Software Engineering, South China University of Technology, Guangzhou, China. He received the Bachelor Degree in Environmental Science and Engineering in 2006 and the Master Degree in Control Science and Engineering in 2009, both from Hunan University in Changsha, China. He received the Ph.D. degree in Computer Science from Nanyang Technological University, Singapore, in 2014. From 2014-2016, he worked as a Senior Research Associate on computer vision in the School of Computer Science, University of Adelaide, Australia. His research interests include machine learning, sparse analysis, deep learning and large-scale optimization.

VII. PROOFS IN SECTION IV

A. Proof of Theorem 1

Theorem 1 Assuming that the distribution of natural data $p(\mathbf{x}) = \mathcal{N}(\boldsymbol{\mu}_x, \sigma_x^2 \mathbf{I})$, where \mathbf{I} is an identity matrix, given a PF ODE sampling $d\mathbf{x} = -t\nabla_{\mathbf{x}} \log p_t(\mathbf{x})$ with $\mathbf{f}(\mathbf{x}, t) = \mathbf{0}$ and $g(t) = \sqrt{2t}$, then for $\forall \mathbf{x} \in p(\mathbf{x})$ and its adversarial sample $\hat{\mathbf{x}} = \mathbf{x} + \epsilon_a$, we have

$$\mathbf{x}_T - \hat{\mathbf{x}}_T \sim \mathcal{N}(\mathbf{0}, 2\sigma_{cl}^2 \mathbf{I}) + \boldsymbol{\mu}_\epsilon, \quad (16)$$

where $\boldsymbol{\mu}_\epsilon = \left(\mathbb{E}_t \frac{t}{\sigma_x^2 + t^2} - 1 \right) \epsilon_a$ and $\sigma_{cl}^2 = \mathbb{E}_t \frac{t^2}{\sigma_x^2 + t^2}$.

Proof. Starting from the PF ODE sampling equation, we derive the corresponding forward ODE:

$$d\mathbf{x} = t\nabla_{\mathbf{x}} \log p_t(\mathbf{x}). \quad (17)$$

We then discretize this equation:

$$\mathbf{x}_{t+\Delta t} = \mathbf{x}_t + t\nabla_{\mathbf{x}} \log p_t(\mathbf{x})\Delta t. \quad (18)$$

Following [15], with $\mathbf{f}(\mathbf{x}, t) = \mathbf{0}$ and $g(t) = \sqrt{2t}$, we have $p(\mathbf{x}_t | \mathbf{x}) = \mathcal{N}(\mathbf{x}, t^2 \mathbf{I})$, which can be derived using Ito calculus [90]. Note that we do not perform this equation to directly obtain the diffused latent vector, *i.e.*, $\mathbf{x}_T = \mathbf{x} + T\mathbf{z}$, where $\mathbf{z} \sim \mathcal{N}(\mathbf{0}, \mathbf{I})$. This single-step diffusion approach does not adequately capture the distribution discrepancy between the latent vectors of adversarial and clean samples. Instead, we aim to explore this distribution discrepancy through a more detailed process using the score function. To this end, we next calculate the score function $\nabla_{\mathbf{x}} \log p_t(\mathbf{x})$.

For the clean sample \mathbf{x} , we have $\mathbf{x}_t = \mathbf{x} + t\mathbf{z} = \mathcal{N}(\boldsymbol{\mu}_x, (\sigma_x^2 + t^2)\mathbf{I})$, yielding

$$\nabla_{\mathbf{x}} \log p_t(\mathbf{x}) = -\frac{\mathbf{x}_t - \boldsymbol{\mu}_x}{\sigma_x^2 + t^2} = -\frac{1}{\sqrt{\sigma_x^2 + t^2}} \mathcal{N}(\mathbf{0}, \mathbf{I}). \quad (19)$$

For the adversarial sample $\hat{\mathbf{x}}$, we have $\hat{\mathbf{x}}_t = \mathbf{x} + \epsilon + t\mathbf{z} = \mathcal{N}(\boldsymbol{\mu}_x, (\sigma_x^2 + t^2)\mathbf{I}) + \epsilon_a$, leading to

$$\nabla_{\hat{\mathbf{x}}} \log p_t(\hat{\mathbf{x}}) = -\frac{\hat{\mathbf{x}}_t - \boldsymbol{\mu}_x}{\sigma_x^2 + t^2} = -\frac{1}{\sqrt{\sigma_x^2 + t^2}} \mathcal{N}(\mathbf{0}, \mathbf{I}) - \frac{\epsilon_a}{\sigma_x^2 + t^2}. \quad (20)$$

Summing Eqn. (18) from $t = 0$ to $t = T$ and setting $\Delta t = 1/T$, $t \in \{0, \frac{1}{T}, \dots, \frac{T-1}{T}\}$, we get

$$\begin{aligned} \mathbf{x}_T &= \mathbf{x}_0 + \frac{1}{T} \sum_{t=0}^1 t \nabla_{\mathbf{x}} \log p_t(\mathbf{x}) \\ &= \mathbf{x}_0 + \frac{1}{T} \sum_{t=0}^1 \mathcal{N}\left(\mathbf{0}, \frac{t^2}{\sigma_x^2 + t^2} \mathbf{I}\right) \\ &= \mathbf{x}_0 + \mathcal{N}\left(\mathbf{0}, \frac{1}{T} \sum_{t=0}^1 \frac{t^2}{\sigma_x^2 + t^2} \mathbf{I}\right) \end{aligned} \quad (21)$$

As $\Delta t \rightarrow 0$ (*i.e.*, $T \rightarrow \infty$), Eqn. (21) converges to:

$$\mathbf{x}_T = \mathbf{x}_0 + \mathcal{N}(\mathbf{0}, \sigma_{cl}^2 \mathbf{I}), \quad (22)$$

where $\sigma_{cl}^2 = \mathbb{E}_t \frac{t^2}{\sigma_x^2 + t^2}$.

Similarly, for adversarial sample $\hat{\mathbf{x}}$, we have

$$\hat{\mathbf{x}}_T = \hat{\mathbf{x}}_0 + \mathcal{N}(\mathbf{0}, \sigma_{cl}^2 \mathbf{I}) - \mathbb{E}_t \frac{t\epsilon_a}{\sigma_x^2 + t^2}, \quad (23)$$

Combing Eqn. (22) and Eqn. (23), we conclude:

$$\mathbf{x}_T - \hat{\mathbf{x}}_T \sim \mathcal{N}(\mathbf{0}, 2\sigma_{cl}^2 \mathbf{I}) + \boldsymbol{\mu}_\epsilon, \quad (24)$$

where $\boldsymbol{\mu}_\epsilon = \left(\mathbb{E}_t \frac{t}{\sigma_x^2 + t^2} - 1 \right) \epsilon_a$. \square

Remark 2. Note that the coefficient $\mathbb{E}_t \frac{t}{\sigma_x^2 + t^2} - 1$ in $\boldsymbol{\mu}_\epsilon$ can be further simplified as $\frac{1}{2} \ln(1 + \frac{1}{\sigma_x^2}) - 1$, which means the coefficient $\mathbb{E}_t \frac{t}{\sigma_x^2 + t^2} - 1 = 0$ if and only if $\sigma_x^2 = 1/99$. However, this is unlikely in practice, as the nature data distributions typically exhibit not only larger but also diverse σ_x values, making such a narrow variance quite rare.

B. Proof of Proposition 1

Proposition 1 Given a test sample $\hat{\mathbf{x}}$, it holds that optimizing a set of latent vectors $\{\tilde{\mathbf{z}}_i\}_{i=1}^K$ by Eqn. (9) gives an upper bound on the reconstruction for the clean sample \mathbf{x} :

$$\frac{1}{K} \sum_{i=1}^K \|f_\theta(\tilde{\mathbf{z}}_i) - \mathbf{x}\|_1 + \beta \mathcal{L}_d(\tilde{\mathbf{z}}) \leq C + \mathcal{L}_a(\tilde{\mathbf{z}}, \hat{\mathbf{x}}) + \beta \mathcal{L}_d(\tilde{\mathbf{z}}), \quad (25)$$

where C is a constant related to the adversarial perturbation.

Proof. Based on the adversarial sample $\hat{\mathbf{x}} = \mathbf{x} + \epsilon_a$, we have

$$\begin{aligned} &\frac{1}{K} \sum_{i=1}^K \|f_\theta(\tilde{\mathbf{z}}_i) - \mathbf{x}\|_1 + \beta \mathcal{L}_d(\tilde{\mathbf{z}}) \\ &= \frac{1}{K} \sum_{i=1}^K \|f_\theta(\tilde{\mathbf{z}}_i) - \hat{\mathbf{x}} - \epsilon_a\|_1 + \beta \mathcal{L}_d(\tilde{\mathbf{z}}) \\ &\leq \|\epsilon_a\|_1 + \frac{1}{K} \sum_{i=1}^K \|f_\theta(\tilde{\mathbf{z}}_i) - \hat{\mathbf{x}}\|_1 + \beta \mathcal{L}_d(\tilde{\mathbf{z}}) \\ &\leq \|\epsilon_a\|_1 + \frac{1}{K} \sum_{i=1}^K \|f_\theta(\tilde{\mathbf{z}}_i) - \hat{\mathbf{x}}\|_1 \\ &\quad + \alpha(1 - \text{SSIM}(f_\theta(\tilde{\mathbf{z}}_i), \hat{\mathbf{x}})) + \beta \mathcal{L}_d(\tilde{\mathbf{z}}) \\ &= \|\epsilon_a\|_1 + \alpha + \mathcal{L}_a(\tilde{\mathbf{z}}, \hat{\mathbf{x}}) + \beta \mathcal{L}_d(\tilde{\mathbf{z}}) \\ &= C + \mathcal{L}_a(\tilde{\mathbf{z}}, \hat{\mathbf{x}}) + \beta \mathcal{L}_d(\tilde{\mathbf{z}}), \end{aligned} \quad (26)$$

where $C = \|\epsilon_a\|_1 + \alpha$. \square

VIII. MORE VISUALIZATION RESULTS

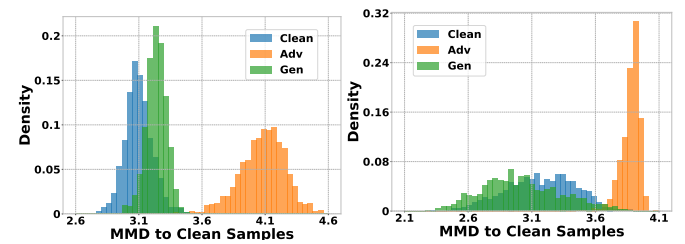


Fig. 7. More histograms cases of MMD distances [17] between the features of clean (Cln) and clean samples *v.s.* generated (Gen) and clean samples *v.s.* adversarial (Adv) samples and clean samples on CIFAR-10 and ImageNet. Both diffusion Model [89] and generative adversarial network [91] are considered, showing the common characteristics of different generative domains.



Fig. 8. Visualization of the perceptual consistency restoration process using different generative models and optimization objectives. The optimization of latent vectors with a generative adversarial network (BigGAN [92]) (**first row in (a)**) typically results in images that exhibit structural blurriness and artifacts. Furthermore, when employing only L1 loss as the alignment loss (**second row in (a), first row in (b)**), the generated samples predominantly preserve overall color and brightness, lacking structural details. In contrast, our CMAP successfully generates refined and fidelity images (**third row in (a), second row in (b)**).